1. Variability of the Oceans

Jin-Yi Yu, Edmo Campos, Yan Du, Tor Eldevik, Sarah T. Gille, Teresa Losada, Michael J. McPhaden, and Lars H. Smedsrud

1.1 Introduction

Oceans have a huge capability to store, release, and transport heat, water, and various chemical species on timescales from seasons to centuries. Their transports affect global energy, water, and biogeochemical cycles and are crucial elements of Earth's climate system. Ocean variability, as represented for example by sea surface temperature (SST) variations, can result in anomalous diabatic heating or cooling of the overlying atmosphere, which can in turn alter the ocean thermal structure and circulation thereby modifying the original SST variations. Climate variations in one ocean basin can propagate to remote basins where they can trigger coupled atmosphere-ocean processes, which themselves propagate raising the possibility of significant interbasin interactions. The present chapter reviews the defining aspects of the climate in individual ocean basins, including mean states, seasonal cycles, and interannual-to-interdecadal variability. Key observational arrays in the tropical oceans are also described.

1.2 Pacific Ocean

The Pacific Ocean extends from the Arctic Ocean in the north to the Southern Ocean in the south and is bounded by Asia and Australia in the west and the Americas in the east (Figure 1.2.1). Major features include wind driven circulations in the subtropical gyres of the North and South Pacific and the subpolar gyre in the North Pacific. The clockwise circulation of the North Pacific subtropical gyre consists of the strong western boundary Kuroshio Current, the westerly-driven North Pacific Current, the eastern boundary California Current, and the trade wind-driven North Equatorial Current (NEC). The clockwise circulation of the North Pacific subpolar gyre is seen north of 50°N, which includes the eastward flowing North Pacific Current, the poleward and westward flowing Alaska and Aleutian Currents, and the southward flowing Oyashio Current. In the South Pacific, the subtropical gyre

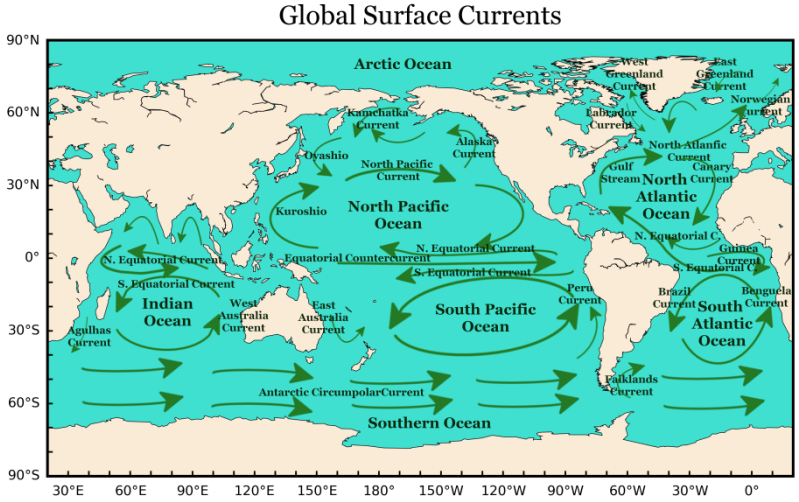

Figure 1.2.1 A schematic of global surface currents.

consists of the East Australian Current to the west, the Peru Current to the east, the eastward South Equatorial Current (SEC) to the north, and the Antarctic Circumpolar Current (ACC) to the south. The complex system of equatorial currents is further discussed in other chapters.

1.2.1 Seasonal cycle of SST

The Pacific Ocean exhibits prominent large-scale variations in SST on timescales ranging from seasonal to interdecadal as well as long-term trends. One outstanding example of SST variability on seasonal time scales is the seasonal cycle of the cold tongue in the tropical eastern Pacific. In here, the annual cycle of SST is stronger than in any other part of the tropics (Kessler et al., 1998). The local seasonal variations are dominated by the annual harmonic with values higher than their annual mean from January through June and lower from July through December, even though the sun crosses the equator twice a year (e.g., Li and Philander, 1996; Yu and Mechoso, 1999). In contrast, in the tropical western Pacific, SSTs are dominated by the semi-annual components and temperatures warm up and cool down twice a year. Another major feature of the SSTs in the tropical eastern Pacific is a pronounced inter-hemispheric asymmetry, with cooler temperatures in the Southern Hemisphere than in the Northern Hemisphere (Philander et al., 1996; McPhaden et al., 2008).

The atmosphere in the tropical eastern Pacific features the Inter Tropical Convergence Zone (ITCZ). This does not follow the sun to the Southern Hemisphere during boreal winter but remains north of the equator. The inter-hemispheric asymmetry of the local SSTs discourages the formation of a southern ITCZ (Ma et al., 1996) though an analogue exists in the form of the South Pacific Convergence Zone which is more strongly developed in the western Pacific (Kiladis et al., 1989). Ocean-atmosphere coupling processes are particularly critical for the variability of the cold tongue-ITCZ complex in the region, where the thermocline depth is shallow and ocean advection has a strong influence on SSTs.

1.2.2 Interannual variability

El Niño and the Southern Oscillation. On interannual timescales, El Niño and its opposite phase La Niña represent the most prominent mode of Pacific Ocean variability (Figure 1.2.2a). El Niño and La Niña are warming and cooling events, respectively, which occur every 2-7 years in the tropical eastern-to-central Pacific (Rasmusson and Carpenter, 1982). El Niño events typically begin in boreal spring, develop in summer and fall, peak in winter, and decay in the following spring. These ocean variation events are accompanied with seesaw fluctuations in sea-level pressures over the southern Pacific and Indian Oceans, which are referred to as the Southern Oscillation (SO; Bjerknes, 1969). The coupling between the oceanic (i.e., El Niño and La Niña) and atmospheric (i.e., the SO) anomalies and the positive feedback between them enables the El Niño/Southern Oscillation (ENSO) phenomenon to grow to strong intensities to profoundly impact climate worldwide.

Since Bjerknes (1969) first recognized the coupled nature of ENSO, extensive effort has been expended by the research community for an improved description, understanding, and prediction. These studies have resulted in novel theories that succeed in explaining many features of ENSO. Chapter 3 reviews outstanding aspects of these theories. They also resulted in the development of numerical climate models that can reasonably simulate and predict ENSO events (e.g., Neelin et al., 1998; Latif et al., 1998).

However, ENSO events since the 1990s have been noticeably different from those in earlier decades (e.g., Kao and Yu, 2009; Lee and McPhaden, 2010; Yu et al., 2012a; Capotondi et al., 2015). El Niño in recent decades tends to develop more frequently in the tropical central Pacific near the International Dateline (Figure 1.2.2b). Such events are referred to as a Central Pacific (CP) El Niño (Kao and Yu 2009), Dateline El Niño (Larkin and Harrison, 2005), El Niño Modoki (Ashok et al., 2007), or Warmpool El Niño (Kug et al., 2009). The canonical El Niño events (Rasmusson and Carpenter, 1982) that start from the South American Coast are referred to as the Eastern Pacific (EP) El Niños (Kao and Yu, 2009; Figure 1.2.2a). The CP and EP types of ENSO produce different teleconnections through the atmosphere and impact global climate in different ways (e.g., Larkin and Harrison, 2005; Ashok et al., 2007; Yu et al., 2012b). The recent change in the ENSO type may be due to background state changes in the tropical Pacific that are either caused by anthropogenic warming (Yeh et al., 2009; Kim and Yu, 2012) or as part of decadal/multi-decadal variability related to Pacific Decadal Oscillation or Atlantic Multidecadal Oscillation (McPhaden et al., 2011; Yu et al., 2015a), although random fluctuations have also been suggested as a plausible reason for changes in ENSO type on decadal timescales (Newman et al., 2011).

El Niño disturbs Walker circulations to induce warming in the tropical Indian Ocean and the tropical North Atlantic Ocean about 3-6 months after its peak (e.g., Lau and Nath, 1996; Klein et al., 1999; Alexander et al., 2002; Cai et al., 2019). It also excites atmospheric wave trains into middle and high latitudes of both hemispheres to remotely influence precipitation and temperature patterns over continents, especially North and South America (e.g., Ropelewski and Halpert, 1986; Karoly, 1989; Mo, 2000), as well as the Arctic polar vortex configuration (e.g., Sassi et al., 2004; García-Herrera et al., 2006; Manzini et al., 2006), Southern Ocean SSTs (e.g., Ciasto and Thompson, 2008; Yeo and Kim, 2015), Antarctic sea ice concentrations (e.g., Liu et al., 2004; Stammerjohn et al., 2008; Yuan and Li, 2008), and Antarctic surface air temperatures (e.g., Kwok and Comiso, 2002; Ding et al., 2011; Schneider et al., 2012). The details of these impacts can be different between the EP and CP types of El Niño.

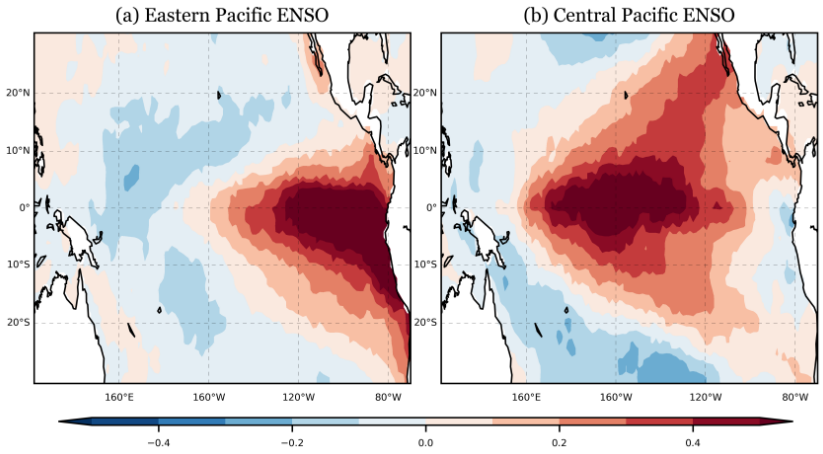

Figure 1.2.2 SST anomaly patterns for the (a) Eastern Pacific (EP) and (b) Central Pacific (CP) types of El Niño obtained from the EOF-regression method of Kao and Yu (2009). SST data from HadISST (1958-2014) is used for the calculation.

The Pacific Meridional Mode (PMM). This is a leading mode of interannual variability in the northeastern Pacific and is characterized by co-variability in SST and surface wind (Figure 1.2.3). Wind fluctuations associated with extratropical atmospheric variability, particularly those linked with the

North Pacific Oscillation (NPO; Walker and Bliss, 1932; Rogers, 1981; Linkin and Nigam, 2008), induce SST anomalies in the subtropical Pacific via surface evaporation. The SST anomalies then feedback on the atmosphere to modify the winds via convection, which tends to produce the strongest wind anomalies to the southwest of the subtropical SST anomalies (Xie and Philander 1994), where new SST anomalies can be formed through anomalies in evaporation. The atmosphere then continues to respond to the new SST anomalies by producing wind anomalies further southwestward. Through this wind-evaporation-SST (WES) feedback (Xie and Philander 1994), the SST anomalies initially induced by the extratropical atmosphere can extend southwestward from near Baja California toward the tropical central Pacific to form the spatial pattern of the PMM (see Chapter 3).

The PMM tends to reach its strongest intensity in boreal spring. Studies have found a strong association between the spring PMM index and the subsequent winter ENSO index (Chang et al., 2007). About 70% of El Niño events occurring between 1958 and 2000 were preceded by SST and surface wind anomalies resembling the PMM. The PMM was suggested to trigger ENSO events either by exciting equatorial ocean waves that propagate toward the eastern Pacific when the PMM wind anomalies arrive at the equator (e.g., Alexander et al., 2010), or by directly increasing the ocean heat content in the equatorial Pacific via modulations in the strength of the trade winds (Anderson 2004). Some studies consider the PMM particularly important in triggering the CP types of ENSO (e.g., Yu et al., 2010; Yu et al., 2017; Yang et al., 2018; Yu and Fang, 2018). The PMM and its associated subtropical Pacific coupling can be a key source of complexity in ENSO evolution (Yu and Fang, 2018).

In the southeastern Pacific, there exists a Southern Hemispheric analogue of the PMM, which is termed the southern PMM. This is also characterized by co-variability in SST and trade wind anomalies extending from the Peruvian Coast toward the equatorial central Pacific. The southern PMM can influence the deep tropics through its connection with cold tongue ocean dynamics to impact the

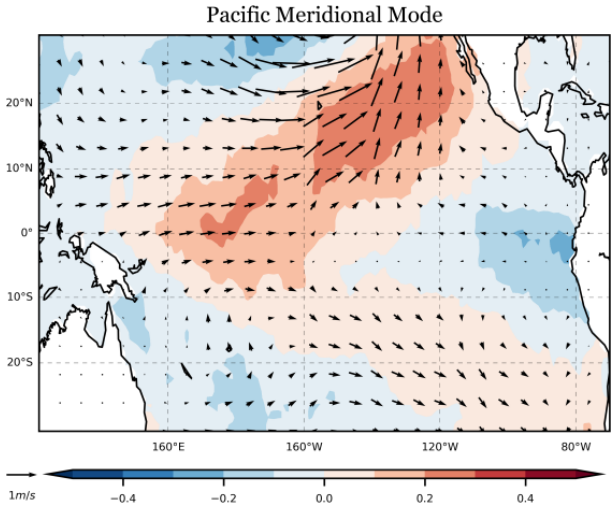

Figure 1.2.3 SST (contours) and surface wind (vectors) anomalies regressed onto the PMM index using HadISST and NCEP-NCAR reanalysis data during period 1958-2014.. The PMM index is from http://www.aos.wisc.edu/~dvimont/MModes/Home.html

development of the EP ENSO (Zhang et al., 2014; You and Furtado, 2017).

Besides influencing the ENSO onset, the PMM can also modulate the occurrence of western Pacific typhoon and eastern Pacific hurricane and precipitation patterns in East Asia and South America (e.g., Li et al., 2011; Murakami et al., 2017; Zhang et al., 2016, 2017).

1.2.3 Interdecadal variability

On decadal or interdecadal timescale, the PDO (Zhang et al., 1997; Mantua et al., 1997) (or the closely related Interdecadal Pacific Oscillation; England et al., 2014) is the most prominent SST variability feature in the Pacific Ocean. It is characterized by a horseshoe pattern of SST anomalies in the tropical eastern Pacific together with SST anomalies with opposite polarity in the central North Pacific. The PDO is suggested to have dominant periodicities in the 50-70 year and bi-decadal year bands (Minobe 1999). During the period of reliable instrumental records, the PDO shifted its phase twice: from a negative to a positive phase around 1976–77 and back to a negative phase around 1999–2000. Around the time of these shifts, significant changes occurred in the Pacific and other basins. The PDO was initially considered to be a physical mode of climate variability that results from atmosphere–ocean coupling within the North Pacific (e.g., Latif and Barnet 1994; Alexander and Deser 1995) or extratropical-tropical interactions (Gu and Philander, 1997). More recent views consider it not a single physical mode but a combination of several processes operating on various time scales (Newman et al., 2016). Ocean circulation patterns associated with the PDO involve changes in the subtropical cells (McCreary and Lu, 1994) and affect equatorial upwelling on decadal time scales (McPhaden and Zhang, 2002, 2004).

1.3 Atlantic Ocean

The Atlantic Ocean is connected with the Arctic Ocean and the Nordic Seas to the North, and the Southern Ocean to the south. Its most important wind-driven circulations are the subtropical gyres in the North and South Atlantic and the subpolar gyre in the north (see Figure 1.2.1).

The North Atlantic subtropical gyre is formed by the strong western boundary Gulf Stream and North Atlantic currents, and the eastern boundary Canary Current Upwelling System. The NEC closes the gyre north of the equator. North of 40N, the North Atlantic Current (NAC) conforms to the southern edge of the subpolar gyre, which is closed by the western East Greenland and Labrador currents. The two northern gyres are connected through the NAC (Talley et al., 2011). The South Atlantic subtropical gyre's major currents are the western boundary Brazil Current, the Benguela current in the eastern boundary upwelling system, the SEC to the north, and the ACC to the south (Talley et al., 2011). When the SEC reaches the South American coast, part of it diverges northward into the North Brazil Current. The complex system of equatorial currents is further discussed in Chapter 3.

The North Atlantic Ocean is one of the sources of deep-water formation in the global oceans, creating an overturning circulation that increases the transport of water and heat from the tropical regions to the north Atlantic sector, resulting in a cross-equatorial northward transport or heat from the South Atlantic Ocean.

1.3.1 Seasonal cycle

The seasonal cycle is the dominant component in the variability of the tropical Atlantic Ocean. This important component is highly coupled with the atmosphere and affected by the shape of surrounding

continents (Li and Philander 1997; Okumura and Xie, 2004). The most important feature of the seasonal cycle of the tropical Atlantic is the development of a tongue of cold SSTs from April to July, followed by a warming over a period that is almost three times longer. SSTs in the equatorial Atlantic band are highest in the boreal spring, when the solar irradiation is maximum in the tropics and the trade winds are weakest. Also in this season, the thermocline is deeper in the east, and the ITCZ is located at the equator above the band of maximum SSTs. Starting in April, the trade winds intensify, and a positive zonal pressure gradient develops along the equator, while SSTs in the eastern Atlantic, cool down and the thermocline shoals. The cooling is maximum in the boreal summer, when a well-developed cold tongue appears south of the equator. As the tropical Atlantic cools down, the oceanic ITCZ moves north following the maximum SST band. The formation of the cold tongue is tightly related to the onset and development of the West African Monsoon. From boreal spring, solar irradiation heats the African continent north of the equator, establishing a meridional gradient of surface pressure along the zonally oriented coast with the equatorial Atlantic that produces an enhancement of the ocean-to-continent southerly winds. These winds induce ocean upwelling and cool the eastern equatorial Atlantic Ocean, which, in turn, further intensifies the southerly winds and the West African monsoon (Okumura and Xie 2004; see Chapter 7).

1.3.2 Interannual variability

Interannual changes can occur in the timing and strength of the seasonal cycle of the tropical Atlantic. These are determined by changes in regional interactions between the ocean and atmosphere and can be excited from sources outside the tropical Atlantic, such as ENSO (Enfield and Mayer 1997). Such interannual variations can have strong influences on regional climate, impacting precipitation, winds and convection, producing changes in the atmospheric circulation that can excite teleconnection patterns and affect distant regions.

During recent decades, the Atlantic Ocean has attracted increased recognition as an important driver of the climate system and its variability. This is apparent in the growing literature focused on the region and in the recent efforts aimed at building a more complete Atlantic observing system. Climate variability in the tropical Atlantic strongly influences the climate of the surrounding continents, affecting winds, precipitation and temperature, and having important impacts on society through changes in hurricane activity and marine productivity. Likewise, the Atlantic Ocean is strongly influenced by other components of the climate system. Moreover, there are intricate links between the interannual variability of the Atlantic Ocean and the other ocean basins, as well as with slow changes in the background state in which the interannual variability is embedded.

Early reviews (e.g., Marshall et al. 2001) described the variability of the North Atlantic climate as a combination of three main components: (1) Tropical Atlantic Variability (TAV), (2) the North Atlantic Oscillation (NAO), and (3) the Atlantic Meridional Overturning Circulation (AMOC). More recently, the multidecadal variability of North Atlantic SSTs, i.e. the Atlantic Multidecadal Variability (AMV), has also become a focal point for research. The following subsections introduce these components and their more important climate signatures. Other chapters in the book present more in-depth discussion of these topics.

The Atlantic Niño. The first mode of interannual variability in the tropical Atlantic is known as the Equatorial Mode, the Zonal Mode or the Atlantic Niño. The pattern of SST anomalies associated with

this mode shows maximum loadings in the eastern equatorial Atlantic that peak in boreal summer (Figure 1.3.1a). It has been established that the dynamics of the Atlantic Niño are similar to the Pacific ENSO (Zebiak, 1993), in which the Bjerknes feedback (Bjerknes, 1969) is crucial. In a positive event, warm SST anomalies in the eastern equatorial Atlantic extend to the south along the African coast, weaker trade winds develop in the western part of the basin and the thermocline deepens in the east (Keenlyside and Latif, 2007; Deppenmeier et al., 2016). The opposite occurs for a negative event. These changes occur through the propagation of equatorial Kelvin and Rossby waves (Polo et al., 2008). Nevertheless, recently some works have alluded to a thermodynamic mechanism triggered by stochastic atmospheric fluctuations as a controlling factor for the development of the Atlantic Niño (Nnamchi et al., 2015, 2016). The relative importance of dynamics versus thermodynamics in the generation of this mode is thus controversial at the present time, although the current consensus is that the dynamical mechanisms are dominant (Jouanno et al., 2017; Dippe et al., 2017).

The Atlantic Niño has direct impacts on the West African Monsoon (WAM) system. The positive phase is associated with a southward migration of the ITCZ, delaying the onset of the WAM and increasing rainfall over the coast of Guinea (Sultan and Janicot, 2003; Okumura and Xie 2004; Rodríguez-Fonseca et al., 2011, 2015). In contrast, the southward migration of the ITCZ results in increased precipitation over Northeast Brazil (Mechoso and Lyons, 1988; Mechoso et al., 1990; Torralba et al., 2015). Outside the tropical Atlantic, it has been shown that the Atlantic Niño can alter the atmospheric circulation of

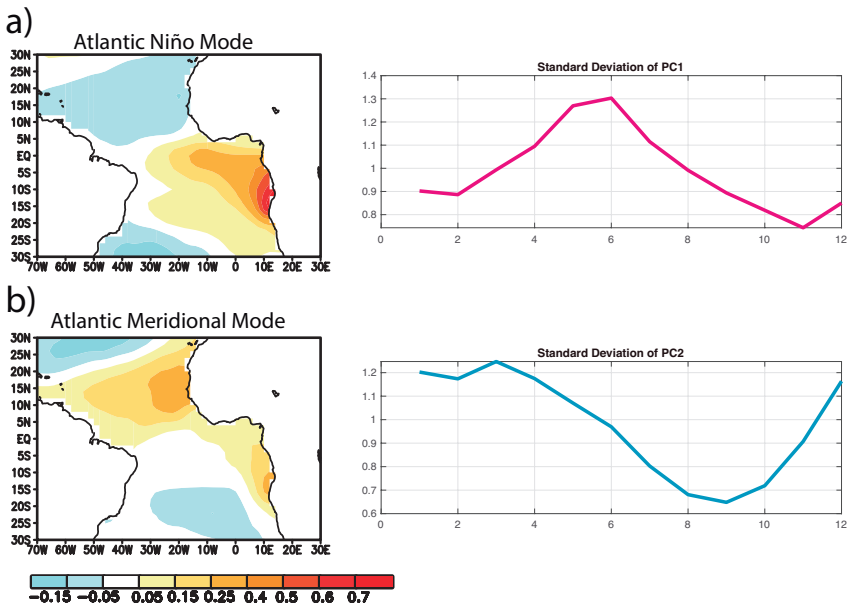

Figure 1.3.1 Dominant modes of variability in the tropical Atlantic Ocean. First (a) and second (b) EOFs of the monthly tropical Atlantic SSTs averaged between 30S-30N and 70W-20E. The modes were calculated from ERSSv3.b dataset (Smith et al., 2008) for the period 1854-2014, using a 13-year high pass filter. All year months were considered for the calculation of the EOF. The year to year standard deviation of the principal components show the seasonality of the modes.

the North Atlantic-European region in summer (Losada et al., 2012) and early winter (Haarsma and Hazeleger, 2007; García-Serrano et al., 2011). The mode also impacts the tropical Indian (Kucharski et al., 2007; 2008; 2009; Losada et al., 2010) and Pacific (Rodriguez-Fonseca et al., 2009; Ding et al., 2012; Martín-Rey et al., 2014; Losada et al., 2010; 2016) Ocean basins.

The Atlantic Niño has been linked to SST anomalies of opposite sign in the subtropical southwestern Atlantic. Nnamchi et al. (2011; 2015) describe the South Atlantic Ocean Dipole (SAOD) as a pattern that presents a dipolar structure, with anomalies of opposite sign in the southwest and northeast of the south Atlantic, the northern pole sharing variability with the Atlantic Niño during certain decades (Nnamchi et al., 2016). According to Nnamchi et al. (2017) the SAOD is the dominant mode of variability in the South Atlantic Ocean and presents common features with the South Atlantic Subtropical Dipole (Venegas et al., 1997). Nevertheless, the characteristics of this mode seem to be strongly determined by the period of study and the treatment of the data, and it is still uncertain if it should be viewed as a separated mode of the Atlantic Niño.

The Atlantic Meridional Mode (AMM). This is the main mode of co-variability between SST and winds in the tropical Atlantic (Nobre and Shukla, 1996; Amaya et al., 2017). The pattern of SST anomalies associated with this mode (Figure 1.3.1b) shows a lobe centered in the subtropical North Atlantic Ocean, around 15N-20W, with peak values in the boreal spring and maximum variability at decadal timescales (Ruiz-Barradas et al., 2000). Chang et al. (1997) argued that the main driver for the generation of this mode in the tropics is the WES feedback. In the positive phase of the AMM, the anomalous warming in the northern subtropical Atlantic is associated with a weakening of the trade winds to the southwest and a strengthening in the northeast. This wind pattern induces heat-flux anomalies that act to extend the SST anomalies further southwest (Ruiz-Barradas et al., 2000). The main mechanism for the generation of the SST anomalies in the northern subtropics is atmospheric forcing by anomalous winter winds (Chiang and Vimont, 2004; Amaya et al., 2017), mainly those associated with ENSO forcing from the Pacific (Enfield and Mayer, 1997) the North Atlantic Oscillation (NAO, Hurrell 1995). There are dynamical linkages between the Atlantic Niño and AAM (Servain et al, 1999; Foltz and McPhaden, 2009) that have important consequences for understanding their regional impacts on climate variability.

The AMM is tightly related to meridional shifts in the position of the ITCZ, which moves towards the warmest hemisphere due to the cross-equatorial boundary layer flow produced by the SST anomalies (Nobre and Shukla, 1996), which affect precipitation over South America and the African continent. In the positive phase of the mode, the ITCZ moves northward, producing droughts over the Northeast region in Brazil (Nobre and Shukla, 1996; Liebmann and Mechoso, 2011). The changes in the subtropical North Atlantic SST also impact the generation of hurricanes whose formation requires warm ocean temperatures and low vertical shears (Kossin and Vimont, 2007).

The North Atlantic Tripole (NAT). This is the main mode of variability in the North Atlantic Ocean. The pattern of SST anomalies associated with this mode consists of a three-lobed structure with anomalies of the same sign in the Northern and Subtropical Atlantic and opposite sign in between. The maximum variability occurs in winter at both interannual and decadal timescales (Deser and Blackmon, 1993). Although ocean dynamics may also have a role in determining the characteristics of this mode, the North Atlantic tripole is fundamentally a response to atmospheric variability through variations in surface stochastic heat fluxes (Fan and Schneider, 2012), which are principally driven by the NAO (Marshall et al., 2001). Although the NAT is primarily an atmospheric forced mode, some studies have suggested that it can affect the circulation at mid-latitudes (Losada et al., 2007).

The North Atlantic Oscillation (NAO). The NAO is the main mode of atmospheric variability in the North Atlantic and can be described as a seesaw of sea level pressure between the Azores high and

the Iceland low (Hurrell, 1995). In its positive phase, enhanced climatological conditions lead to dry conditions in Southern Europe; in its negative phase, weakening climatological conditions result in wet conditions in Northern Europe. As noted above, it is a major driver of ocean variability in the Atlantic.

1.3.4 Multidecadal variability

The main mode of SST variability in the Atlantic Ocean at multidecadal scales is the Atlantic Multidecadal Variability (AMV), also known as Atlantic Multidecadal Oscillation (AMO; Kerr, 2000; Knight 2005). The pattern of SST anomalies associated with this mode shows an oscillation in which the positive phase features warm SST anomalies over the whole North Atlantic with maximum loadings off Newfoundland, and very weak anomalies of opposite sign in the southern Atlantic. The

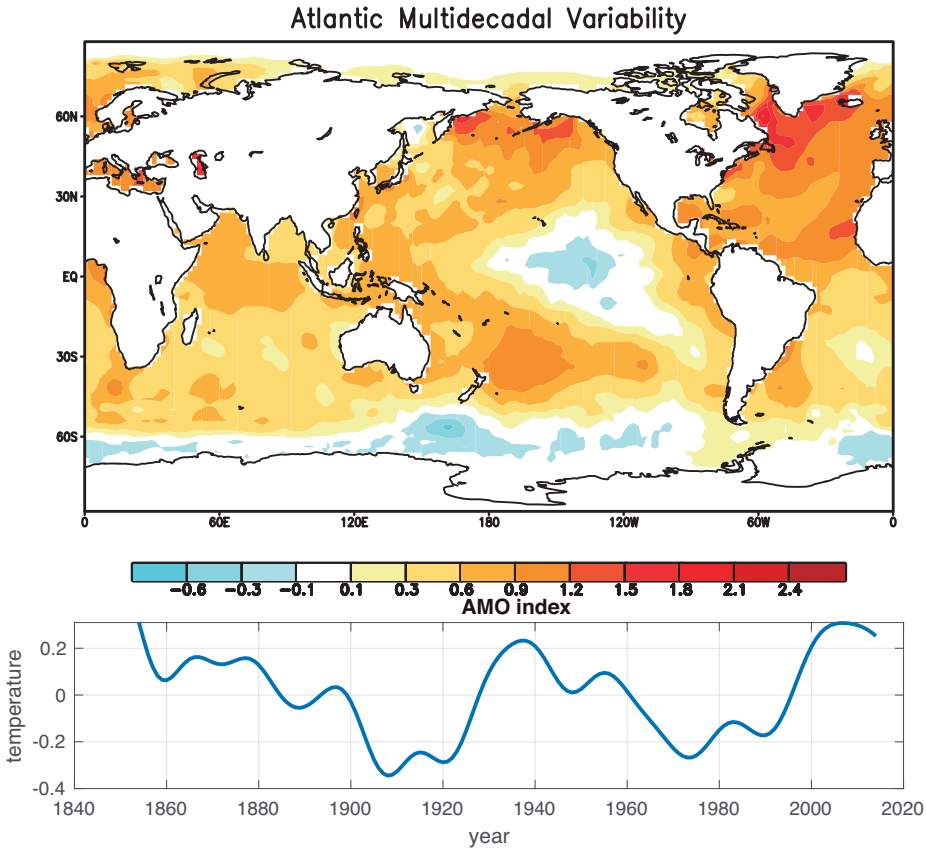

Figure 1.3.2: Regression of the annual global SSTs (top) onto the AMV index (bottom) calculated as the mean SST averaged in the North Atlantic SSTs (0-70N 70W-0E) for the period 1854-2014, using a 13-year low pass filter. SST data comes from ERSSv3.b dataset (Smith et al., 2008).

mode has a periodicity of 60-80 years and amplitude of around 0.4ºC. The SST pattern also projects on the rest of the ocean basins (Figure 1.3.2). The AMV has been identified in paleoclimate studies (Delworth and Greatbach, 2000; Mann et al., 2009; Svendsen et al., 2014). Some works describe a contribution to the mode by the effects of anthropogenic aerosols (Terray, 2012).

Although it is widely accepted that the AMV is tightly related to the decadal variability of the Atlantic Meridional Overturning Circulation (AMOC; Delworth and Mann, 2000; Vellinga and Wood, 2002 Knight 2005), which transport heat to the surface layers of the North Atlantic Ocean, the importance of other factors has also been also explored. In this way, the stochastic forcing of the atmosphere over

the North Atlantic, in particular related to variations in the NAO, has been proposed as an important driver of the AMV (Alexander et al., 2014; Clement et al., 2015; Zhang et al., 2016). The AMV has been receiving more and more attention from climate scientists, and a large amount of literature exists on its impacts on climate. It has been related to tropical hurricane activity that intensifies during positive AMV phases (Goldenberg, 2001; Zhang and Delworth 2006); as well as with the modulation of rainfall in the Sahel (Mohino et al., 2011; Dieppois et al., 2015) and South America (Villamayor et al., 2018) through changes in the interhemispheric gradient of SST and position of the ITCZ (Zhang and Delworth, 2006; Mohino et al., 2011). The AMV has been also linked to changes in the extratropical climate (Enfield et al., 2001; Sutton and Hodson, 2005; Ruprich-Robert et al., 2017, 2018).

Several recent studies have examined the modulation of the interannual variability of climate by low-frequency variability patterns. It has been found that the AMV can modulate the variability of the interannual modes in the tropical Atlantic (Martin-Rey et al., 2018) and teleconnections between remote locations, such as the tropical Pacific El Niño (Levine et al., 2017; Cai et al., 2019) and European precipitation (López-Parages et al., 2012;).

3.5 Atlantic Meridional Overturning Circulation

The circulation of the deep ocean is driven by changes in surface buoyancy at polar regions. The North Atlantic Ocean holds some of the most important sources of deep-water formation, located in the Labrador and Greenland Seas. Cold and salty waters sink in the North Atlantic Ocean and flow towards the Southern Hemisphere in the deep ocean, while warm waters move northward in the surface layers of the ocean. This cell is known as the Atlantic Meridional Overturning Circulation (AMOC) and is a key mechanism for the global redistribution and transport of heat from the Southern to the Northern Hemisphere in the Atlantic. The AMOC makes climate in the North Atlantic-European region gentler, the Northern Hemisphere warmer than the Southern, and affects the main position of the Atlantic ITCZ (Frierson et al., 2013; Marshall et al., 2014; Buckley and Marshall, 2016). The AMOC variations impact climate variability at different timescales (e.g., Delworth et al. 1993; Delworth and Mann, 2000; Knight et al., 2005; Zhang and Delworth, 2005, Danabasoglu et al., 2012), being a main driver of the AMV. It is also a key factor for the redistribution of anthropogenic influences on temperature to the deep ocean (Kostov et al., 2014). In turn, it has been shown that the AMOC is influenced by the NAO through the modification of surface fluxes (Delworth and Greatbatch, 2000), with stronger impact at decadal timescales (Delworth and Zeng, 2016).

1.4 Indian Ocean

The Indian Ocean is bounded by Asia, Africa, Australia, and the Southern Ocean in the south (see Figure 1.2.1). It has a prominent counter-clockwise subtropical gyre in the southern Indian Ocean that consists of the strong western boundary Agulhas Current, and the trade wind-driven SEC, the eastern boundary West Australian Current, and the westerly-driven ACC. In the northern part, upper ocean currents are strongly influenced by the seasonal reversal of winds from summer to winter.

In the interior Indian Ocean, the cross-equatorial cell (CEC) is a wind-driven meridional circulation crossing the Northern and Southern Hemispheres (Miyama et al., 2003; Lee, 2004). The surface branch of the CEC is a southward cross-equatorial Sverdrup transport forced by the integrated zonal wind-stress curl along the equator. The surface water subducts into the thermocline in the subtropical south

Indian Ocean and flows northward to supply the upwelling off Somalia (Schott et al., 2004; Schott et al., 2009; Wang and McPhaden, 2017). The CEC plays an important role on the mass and heat balance of the northern and southern Indian Ocean.

1.4.1 Seasonal cycle

The monsoonal winds over the Indian Ocean north of 10°S vary seasonally, forcing remarkable seasonal variations in ocean currents. During boreal summer, the prevailing Indian Monson winds over the region are southwesterly. The winds drive a clockwise upper ocean circulation that is referred to as the Summer Monsoon Current or Southwest Monsoon Current (SMC). The clockwise SMC in the Arabian Sea flows southeast-ward along the western coast of India, then bends around India and Sri Lanka, and finally turns northward into the Bay of Bengal (Figure 1.4.1). During boreal winter, northeasterly winds prevail over the northern Indian Ocean and drive a counter-clockwise upper ocean circulation that is referred to as the Winter Monsoon Current or Northeast Monsoon Current (NMC). The NMC flows westward from the northwest Bay of Bengal, around India and Sri Lanka, and counter-clockwise in the Arabian Sea (see Figure 1.4.1).

Strong seasonal variations also occur in the NEC and in the Somali Current (SC) near the equator. During the summer monsoon, the prevailing southwest winds producing strong surface currents from west to east and eliminate the NEC. In contrast, the NEC appears during the winter when the northeast monsoon winds strengthen westward currents. The revering monsoon winds also cause the Somali Current (SC) to flow northward during summer but southward during winter (see Figure 1.4.1).

Surface easterlies are not present throughout the year in the equatorial Indian Ocean. Instead, westerlies occur during the transition seasons of the Indian Monsoon (April to May, and, October to November) (Hellerman and Rosenstein, 1983; Schott et al., 2009). The eastward winds force zonal surface currents flowing eastward during both inter-monsoon periods (see Figure 1.4.1), which are commonly referred to as Wyrtki Jets (Wyrtki, 1973; McPhaden et al., 2015). Wyrtki Jets play a key role in the exchange of mass, heat and freshwater between the eastern and western equatorial Indian Ocean.

The Equatorial Undercurrent (EUC) is an eastward zonal flow under a westward or weaker eastward flowing surface current in the equatorial Indian Ocean, with a core near the 20℃ isotherm (Bruce, 1973; Reppin et al., 1999; Iskandar et al., 2009; Chen et al., 2015). The EUC is transient and regularly appears in boreal winter and spring, resulting mainly from equatorial Kelvin and Rossby waves triggered by equatorial easterly winds (Iskandar et al., 2009; Chen et al., 2015).

The Indonesian Throughflow (ITF, Figure 1.4.1; see Chapter 6) provides the only low-latitude pathway for the transfer of warm and low salinity seawater from the Pacific into the Indian Ocean through the Indonesian Seas (Gordon 1986; Hirst and Godfrey, 1993; Gordon, 2005; see Chapter 6)). The mean ITF transport (around 15*Sv*±5*Sv*) varies seasonally, with a maximum transport during boreal summer and a minimum in boreal winter (Meyers et al., 1995). The ITF transport is stronger during the La Niña phase and weaker during the El Niño phase (Liu et al., 2015). Most of the ITF water exits the Indian Ocean through the Leeuwin Current and the Agulhas Current. The Leeuwin Current flows poleward along the west coast of Australia, carrying low-salinity and warm water (Cresswell and Golding, 1980; Thompson, 1984; Domingues et al., 2007; Furue et al., 2013). The current is primarily driven by a large meridional pressure gradient along the western Australian coast set up by the ITF and local air-sea fluxes, thus, providing a pathway for seawater from Pacific into the Indian Ocean's boundary current system (Thompson, 1984; Yit Sen Bull and van Sebille, 2006; Lambert et al., 2016). It has important impacts on the fisheries, marine ecosystems, and regional climate.

1.4.2 Interannual variability

Indian Ocean Basin Mode (IOB). This is the leading mode of interannual SST variability in the tropical

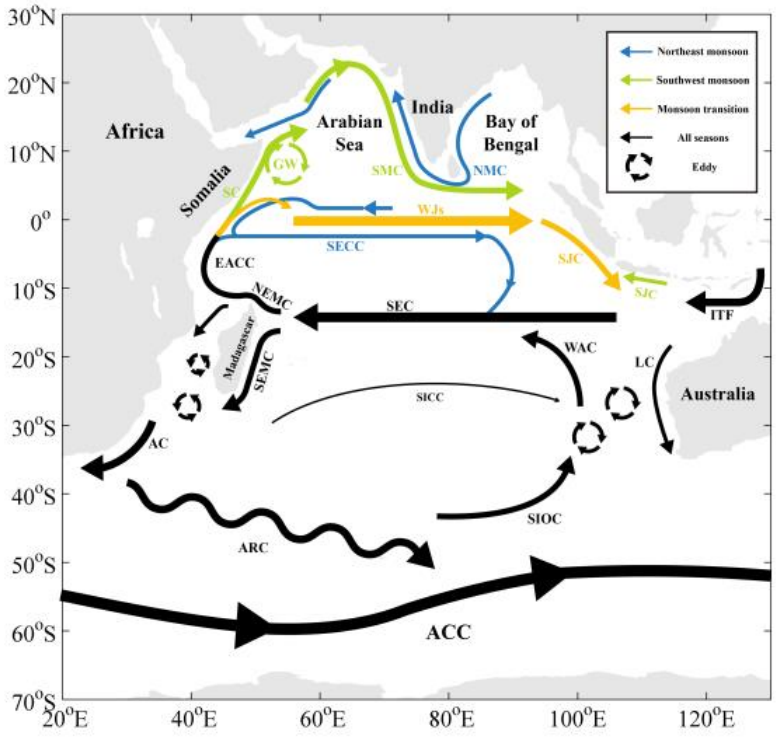

Figure 1.4.1: Schematic diagram of the current system in the Indian Ocean. The acronyms indicate the Indonesian Throughflow (ITF), South Equatorial Current (SEC), South Java Current (SJC), South Equatorial Countercurrent (SECC), South Indian Ocean Countercurrent (SICC), Northeast and Southeast Madagascar Current (NEMC and SEMC), East African Coastal Current (EACC), Wyrtki Jets (WJ), Southwest and Northeast Monsoon Currents (SMC and NMC), Agulhas and Return Current (AC and ARC), Great Whirl (GW), Somalia Current (SC), South Indian Ocean Current (SIOC), Leeuwin Current (LC), and West Australia Current..

Indian Ocean, showing a basin-wide warming or cooling (Figure 1.4.2a). The strength and frequency of the mode are highly related to ENSO. An Indian Ocean basin warming typically peaks in the spring

following an El Niño that matures in winter (e.g., An 2004; Yu and Lau 2004). The IOB warming is largely driven by reduced surface latent heat flux release and increased downward shortwave radiation, except in the southwest Indian Ocean, where Rossby wave-upwelling interactions are important (e.g. Klein et al., 1999; Xie et al., 2002; Du et al., 2009; Izumo et al., 2008).

During the El Niño, anticyclonic wind stress curl anomalies induce oceanic down-welling Rossby waves in the tropical south Indian Ocean. The westward slow-propagating Rossby waves deepen the thermocline, and the southwest tropical Indian Ocean warms up. During the decaying phase of El Niño, in spring and summer, wind anomalies associated with such warming have an asymmetrical pattern about the equator, with northeasterlies in the north and northwesterlies in the south (Wu et al 2008). As mean winds turn southwesterly in late spring over the north Indian Ocean, these force the SST to warm again via reductions in the wind speed and surface evaporation (Du et al., 2009, Wu and Yeh, 2010; Xie et al., 2016). Thus, the north Indian Ocean displays a double-peak warming in which the second peak appears to be stronger and persist into summer (Du et al., 2009).

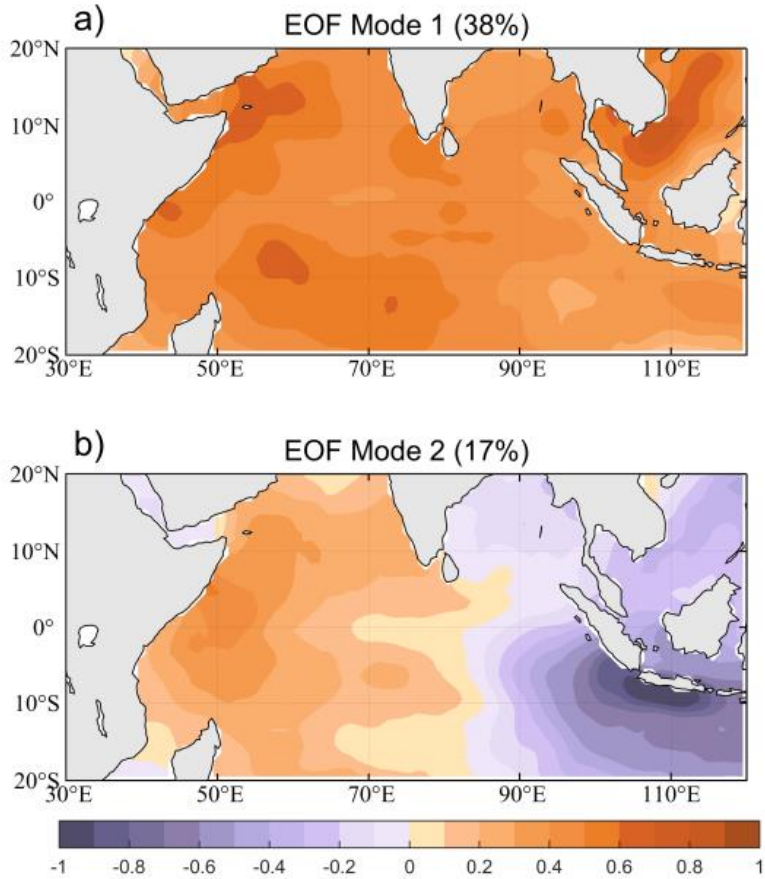

Figure 1.4.2: Empirical Orthogonal Function (EOF) decomposition on monthly SST in the tropical Indian Ocean (30°E -120°E, 20°N-20°S). (a) and (b) show the first and second modes, which indicate the Indian Ocean Basin mode (IOBM) and the Indian Ocean Dipole mode (IOD), with variance contribution 38% and 17%, respectively. The SST data is from Optimum Interpolation Sea Surface Temperature (OISST) dataset during 1982-2017.

The IOB has significant influences on Indo-Pacific climate through modulations of the monsoon north of the equator and atmospheric circulation over the Northwest Pacific in what is known as the Indian Ocean-Pacific Ocean Capacitor effect. The warming forces a warm baroclinic Kelvin wave that propagates eastward into the Western Pacific. Surface friction drives a northeasterly wind into the

equatorial low pressure in the baroclinic Kelvin wave and induces surface convergence on the equator and divergence off the equator thereby triggering suppressed deep convection and anomalous anticyclone over the Northwest Pacific (Xie et al., 2009).

Through modulating the equatorial atmospheric Kelvin wave activity over the Western Pacific, the IOB can significantly affect the duration of El Niño and La Niña events (Okumura and Deser, 2010). The IOB also affects the intensity of the Western Pacific summer monsoon and thereby tropical cyclone genesis and largely determines the number of tropical cyclones in the Northwest Pacific (Zhan et al., 2011; Du et al., 2011). The IOB has important impacts on the distribution of summer air temperature and extreme high temperature disasters in eastern China (Hu et al., 2011; 2013). In addition, it can influence the position and strength of the subtropical high-level jet in East Asia (Qu and Huang et al., 2012). These impacts are generally captured in numerical experiments performed with atmospheric general circulation models (e.g. Xie et al., 2009; Wu et al., 2010; Chen et al., 2016; 2017).

IOB impacts on the Northwest Pacific climate vary with time. Before 1976/77, El Niño-induced warming of the Indian Ocean did not persist through summer and had little effect on the Northwest Pacific anticyclone. However, since 1976/77, the warming has tended to persist through summer, and summertime SST anomalies in tropical Indian Ocean are more likely to trigger Kelvin fluctuations affecting the Northwest Pacific climate (Huang et al., 2010).

The Indian Ocean Dipole (IOD). This mode in the tropical Indian Ocean features a seesaw, zonal structure (Figure 1.4.2b). IOD events typically peak in the boreal autumn (September-October-November). During a positive IOD phase, SSTs cool down in the southeastern region and warm up in the western region (Saji et al., 1999; Webster et al., 1999; Behera et al., 1999; Annamalai et al., 2003). These SST anomalies are associated with surface pressure and wind anomalies over the equatorial region. The easterly wind anomalies lead to oceanic upwelling Kelvin waves that propagate eastward, lifting the thermocline off the Sumatra-Java coast (Yuan and Liu, 2009; Chen et al., 2016; Delman et al., 2016) as a Bjerknes feedback sets off (Bjerknes, 1969). Thus, the IOD is dominated by its eastern pole, which features a positive skewness (Cai and Qiu, 2013; Ng et al., 2014; Zheng et al., 2010).

Before 1999, the IOD was attributed to ENSO impacts. For example, the 1997 positive IOD event was accompanied by one of the strongest El Niños on record (Yu and Rienecker, 1999). However, in 1961 and 1994 the Indian Ocean rim suffered severe extreme weather without a strong ENSO in the Pacific (Behera et al., 1999; Conway, 2002; Vinayachandran et al., 1999). Saji et al. (1999) proposed that the IOD is an intrinsic climate mode in the tropical Indian Ocean, with ENSO as one of the possible triggering mechanisms via both atmospheric and oceanic pathways (atmospheric bridge and oceanic tunnel respectively). A full description of these mechanisms is in Chapter VI. The IOD also shows a quasi two-year variability (Feng and Meyers, 2003; Li et al., 2003; McPhaden and Nagura, 2014). This has been related to the Tropical Biennial Oscillation (TBO) (Meehl and Arblaster, 2001) as well as to ENSO (Li et al., 2003).

The IOD has remarkable climatic impacts in regional and even global scales. Some examples of these impacts are heavy rainfall and extensive flooding in equatorial East Africa (Annamalai et al., 2005; Behera et al., 1999; Conway, 2002; Webster et al., 1999), drought and bushfire in Indonesia and Australia (Cai et al., 2009; Saji et al., 1999; Ummenhofer et al., 2009), and Asian Monsoon intensity (Guan and Yamagata, 2003; Yuan et al., 2008). IOD variability can also feedback on ENSO. This feedback affects the Walker Circulation system and hence the zonal wind anomalies in the tropical

Pacific (Behera and Yamagata, 2003; Kug et al., 2006; Yu et al., 2002; Izumo et al., 2010). Moreover, the oceanic pathway, the Indonesian Seas, also can convey IOD effects to the Pacific. Oceanic dynamics involving SST and sea surface height anomalies propagate eastward from the southeastern tropical Indian Ocean to the eastern tropical Pacific through the Indonesian Seas and affect the cold tongue SST, suggesting a potential role in ENSO predictability (Yuan and Liu, 2009; Yuan et al., 2013; Zhao et al., 2016).

1.4.3 Interdecadal variability

Beyond the interannual time scale, the IOB and the IOD feature low-frequency variations (Han et al., 2014). IOD variability was strong in the 1960s and in the 1990s but weak in the 1980s (Ashok et al., 2004; Yang et al., 2017). Ummenhofer et al. (2017) proposed that the PDO influences IOD decadal variability via the oceanic pathway through the ITF and subsurface Rossby waves across the southern Indian Ocean basin. However, Tozuka et al. (2007) proposed that the duration of a Rossby wave crossing the basin is too short to explain the decadal variability of the IOD, and the southern heat transport may be important. Therefore, the reason for the low-frequency IOD variability is still an open question. Du et al. (2013) classified three kinds of IOD types and proposed an "Unseasonable IOD" based on IOD lifetime, which is independent to ENSO cycle. This unseasonable IOD is related to the Indian Ocean internal variability and only came up after the mid-1970s, suggesting that climate change may affect the IOD characteristics by inducing different SST warming rates in the tropical Indian Ocean. Zhang at al. (2018) further indicated a relationship between the IOD decadal variation thermocline states along the equatorial Indian Ocean, which change the efficiency of thermocline feedback. Links have also been suggested between interdecadal variability of the IOD and the ITF. The latter can be affected by mid-latitude Rossby waves propagating from the subtropical North Pacific from the Pacific through a pathway that was not important before 1980, but which became prominent afterward (Cai, 2005). Decadal variability was also observed in the strength of the Subtropical Cell in the Indian Ocean, which slowed down during 1992-2000 (Lee, 2004) but returned back to the pre-1992 level during 2000-2006 (Lee and McPhaden, 2008).

1.5 Southern Ocean

The Southern Ocean is traditionally defined to encompass the portion of the global ocean south of 30°S or 35°S (see Figures 1.2.1 and 1.5.1). The major current of the Southern Ocean is the Antarctic Circumpolar Current (ACC), which flows eastward around the Antarctic continent, with an average latitude around 50°S, and is driven by the mid-latitude westerly winds. Measurements by Donohue et al (2016) in the Drake Passage indicated that the total transport of the ACC is 173 million $m^3\ s^{-1}$ (173 Sv). The ACC comprises multiple narrow frontal jets, identified from north to south as the Subantarctic Front, the Polar Front, and the Southern ACC Front (e.g. Orsi et al 1995, Figure 1.5.1). Analyses of satellite data indicate that the major fronts can have multiple quasi-stationary positions (Sokolov and

Rintoul, 2009), implying a complex ACC structure, with jets that meander in position and strengthen and weaken over time, depending both on the wind and on the intrinsic instabilities of the system.

1.5.1 Antarctic Circumpolar Current (ACC)

The winds that drive the Southern Ocean have a deep-reaching impact on ACC circulation, despite the fact that wind can only have a direct impact on the ocean in a thin layer within the upper ocean. Winds can help to homogenize the mixed layer, which represents the top most layer of the ocean, typically

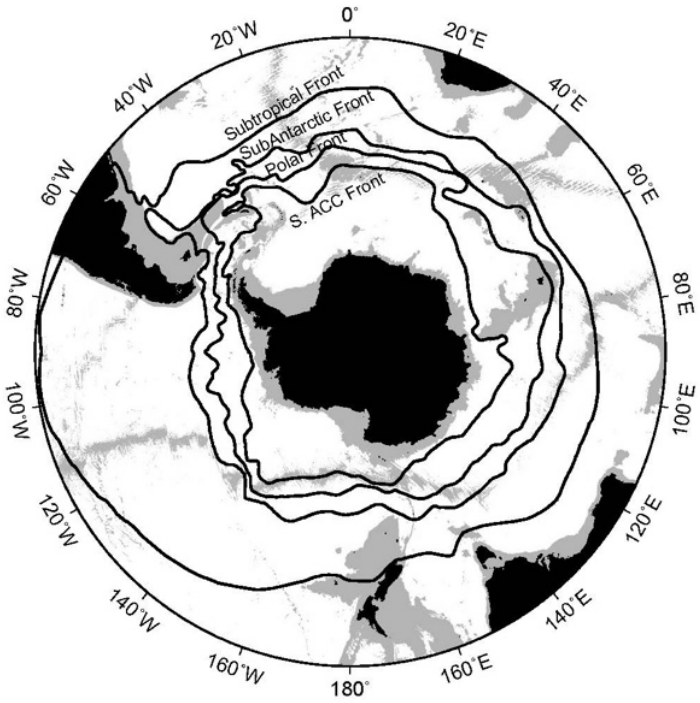

Figure 1.5.1: The positions of the main fronts that define the Antarctic Circumpolar Current (as defined by Orsi et al 1995). Gray shading indicates bathymetry shallower than 3000 m.

less than 100 m deep (although in the Southern Ocean, wintertime buoyancy forcing can lead to much deeper mixed layers). Because of the Earth's rotation, time-mean transport within the so-called Ekman layer in the upper ocean is orthogonal to the wind---northward within the zone of mid-latitude westerlies. This effectively drives water northward in the region of the ACC. The northward Ekman transport has two effects. First, the pile up of water north of the ACC establishes a north--south pressure gradient across the ACC, not just at the surface but throughout the water column, and this supports the top-to-bottom geostrophic transport that characterizes the ACC, sustaining the its large zonal transport. Second, because the mid-latitude winds are centered at approximately the latitude of the ACC, the northward transport of water at the surface necessitates upwelling in the ACC, thus establishing the meridional overturning circulation in the Southern Ocean. In the upper limb of the Southern Hemisphere meridional overturning circulation, water that is advected southward at mid-latitudes upwells along steeply tilted isopycnal surfaces and returns northward as Ekman transport at the surface (e.g. Speer et al, 2000, see Figure 1.5.2). The fact that the winds are strongest over the ACC (which also implies zero wind-stress curl over the ACC) is important: if the winds were uniform

at all latitudes, then the northward Ekman transport would also be uniform and would need to be balanced via coastal upwelling along the Antarctic margin.

The ACC delineates a boundary between mid-latitudes, where temperatures are consistently above freezing, and the Antarctic marginal seas, where wintertime sea ice can readily form. When seawater freezes, the crystal structure of the ice does not include salt, and saltwater brine is rejected from the ice. This cold and salty water is exceptionally dense. It sinks and mixes with the surrounding water, which helps to form the lower limb of the meridional overturning circulation: water advected southward at mid-depth upwells on the southern edge of the ACC, where it mixes with dense cold and salty water, sinks to become Antarctic Bottom Water, and then returns. Because the winds over the ACC make it a region of strong upwelling, it is sometimes thought of as a boundary that blocks warmer mid-latitude waters from coming into contact with the Antarctic marginal seas. The ACC is also a region of strong eddy activity, and eddies can facilitate southward transport of heat. Numerical studies to assess the relative roles of the ACC as a barrier or a blender (e.g. Abernathey et al., 2010; Griesel et al., 2010; Tulloch et al., 2014) have suggested that enhanced or diminished mixing regions can both occur within the core of the ACC.

Processes that occur in Antarctic marginal seas are of global importance. The ice sheets on the Antarctic continents protrude into the ocean as ice shelves, which float on the ocean surface, with ocean water circulating in the sub-glacial cavity below the base of the ice and above the sea floor. When ice shelves melt, the most rapid melting tends to occur on their undersides, so melt rates are

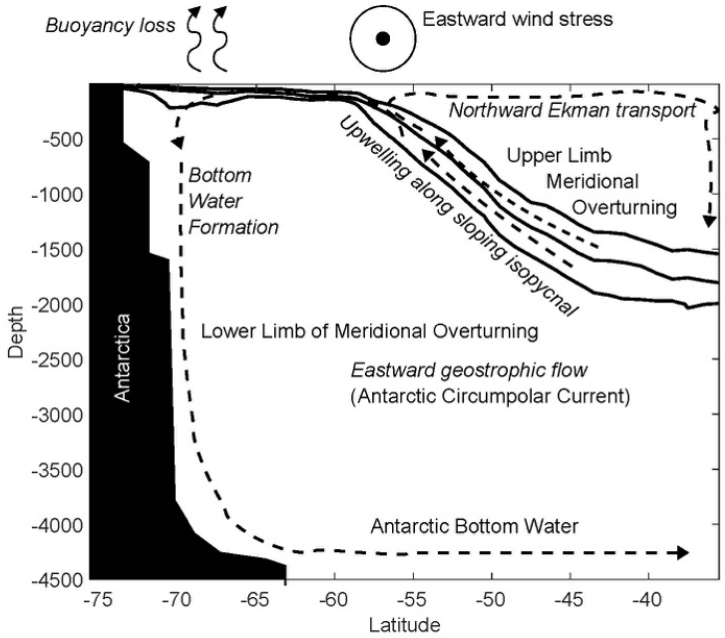

Figure 1.5.2: A schematic showing the Southern Ocean meridional overturning circulation, based on the potential density computed from the World Ocean Atlas 2018, averaged from 180W to 110W. Processes are identified in italics and features in non-italicized text. .

driven by the temperature and rate at which ocean water circulates through the subglacial cavities (e.g. Rignot and Jacobs, 2002; Pritchard et al, 2012). Since ice shelves float, ice shelf melting itself has no direct bearing on global sea level, but in many locations around Antarctica, ice shelves play a critical role in buttressing the ice sheets onto the continent, so rapid ice shelf melt has the potential to

accelerate the motion of ice sheets, resulting in a reduction in total land ice and correspondingly higher global sea level.

The schematic picture of the ACC presented here suggests a zonally uniform system. In reality, the flow is zonally inhomogeneous. The latitude of the ACC fronts varies, reaching the most northerly positions in the Atlantic Ocean, and the most southerly positions in the eastern Pacific just before the flow enters Drake Passage. The ACC turns sharply north just after passing through Drake Passage and navigates through narrow gaps in the Scotia Ridge. All along its path, the ACC is steered by topography. The most significant eddy activity and the largest southward transport are concentrated in a few regions where topography disrupts the zonal flow (e.g. Thompson and Sallée, 2012; Tamsitt et al, 2017). To the south of the ACC, the marginal seas that surround Antarctica also vary with longitude, as different marginal seas have different shapes and are different distances from the ACC. The distance between the ACC and the Antarctic continent is at a minimum in the southeast Pacific, adjacent to the Amundsen Sea. Thus, comparatively warm Circumpolar Deep is expected to circulate readily onto the Antarctic continental shelf and under the ice shelves in the Amundsen Sea. Perhaps not surprisingly, the Amundsen Sea has been identified as a region with some of the most rapidly warming shelf waters around Antarctica (e.g. Schmidtko et al., 2014), rapidly thinning ice shelves (Paolo et al, 2015), and rapid melting of continental ice (e.g. Rignot et al., 2008, 2013).

1.5.2 Southern Annular Mode (SAM)

The Southern Annular Mode (SAM, e.g. Thompson et al, 2000) represents the leading mode of wind variability in the Southern Ocean. It is defined as the first empirical mode of pressure differences between Antarctica and mid-latitudes. As a result of stratospheric ozone depletion (e.g. Baldwin and Dunkerton, 2001; Thompson et al, 2011; Polvani et al, 2011) and greenhouse warming (e.g. Fyfe and Saenko, 2006; Cai, 2006; Cai and Cowan, 2007), the SAM has intensified over the last four decades (Marshall, 2003), which implies stronger winds that are located further south. Since the ACC is a wind-driven current, it is hypothesized to be sensitive to changes in wind forcing. However, long-term climate records and eddy-resolving climate simulations suggest that stronger winds have not accelerated the ACC (e.g. Böning et al, 2008), nor have they led to a clear poleward shift in the latitude of the ACC (e.g. Gille, 2014; Shao et al, 2015). Instead, the intensified SAM is thought to have possibly led to increased eddy activity (e.g. Meredith and Hogg, 2006), potentially supporting increased poleward heat transport by eddies.

ENSO can also influence the Southern Ocean, particularly in the Pacific sector, sometimes in tandem with the SAM, and sometimes out of phase (e.g. Fogt and Bromwich; 2006; Stammerjohn et al., 2008; Yu et al., 2015b). ENSO events can set off circulation patterns in the atmosphere (Karoly, 1989; Mo, 2000) and coastally trapped Kelvin waves in the ocean that propagate southward along the coast of South America. Together, these atmospheric and ocean waves can influence the winds around Antarctica. As a result, El Niño events are associated with warming and increased ice melt in the region of the Antarctic Peninsula (e.g. Ding et al, 2011; Paolo et al, 2018).

While much of the discussion of variability in the Southern Ocean focuses on large-scale climate patterns driven by large-scale winds linked to the SAM and ENSO, local winds can also shape the circulation. In the southeast Pacific, the Amundsen Sea Low strengthens and weakens over time (Raphael et al. 2016) and can further modulate circulation patterns. Detailed analyses of numerical

model output have highlighted the roles of local winds and buoyancy forcing, as well as localized topography and eddies, in governing cross-shelf heat transport around the Antarctic continent (e.g. Stewart and Thompson, 2015; Rodriguez et al, 2016; Palóczy et al, 2018).

1.5.3 The Warming Trend

Long-term observational records provide evidence that the Southern Ocean has warmed and freshened over the last 50 to 100 years (e.g. Gille, 2002; Aoki et al., 2005; Gille, 2008; Böning et al., 2008; Durack et al., 2012). Since the advent of Argo measurements in 2004, the Southern Ocean has emerged as the region of the world's ocean that is undergoing the most rapid increase in vertically integrated heat content (Roemmich et al., 2015). Although there is considerable natural variability in the Antarctic region (e.g. Jones et al, 2016), the warming and freshening have been largely attributed to greenhouse gases, with smaller effects due to ozone depletion (e.g. Swart et al., 2018).

Despite the large-scale warming throughout the water column, satellite sea surface temperature records indicate that surface temperatures have cooled over the last two to three decades (e.g. Armour et al, 2016) and sea ice extent has expanded (e.g. Comiso and Nishio, 2008; Comiso, 2010; Eisenman et al, 2014). Climate simulations suggest that the surface cooling and increased sea ice extent can be explained as a result of an acceleration in the meridional overturning circulation: increased westerly winds lead to increased upwelling of cold deep waters and increased northward Ekman transport (e.g. Armour et al., 2016; Kostov et al., 2016). This advects sea ice and cold water northward, resulting in both colder and fresher surface waters in the ACC region (e.g. Haumann et al., 2016).

1.6 The Arctic Mediterranean

The Arctic Mediterranean comprises the Arctic Ocean and the regional seas confined between Greenland and Norway north of the Greenland-Scotland Ridge (Fig. 1.6.1; Aagaard et al. 1985). The climatic significance of the Arctic Mediterranean can be summarized as follows. It is a main heat source for the atmosphere from oceanic heat convergence and a main receiver of freshwater exported to the North Atlantic Ocean from river runoff and net precipitation (Ganachaud and Wunsch 2000; Peterson et al. 2006; Eldevik and Nilsen 2013). Its role in the planetary cycling of heat and freshwater is particularly pronounced when considering its relatively small size for a world ocean. With the dominant presence both of the Arctic cryosphere and the Gulf Stream's northernmost limb, regional climatic contrasts are large and air-ice-ocean interactions are forceful, plentiful and multifaceted (Smedsrud et. al 2013; Vihma 2014). This section focuses on the Arctic sea ice and its variability, while Chapter 10 gives a more comprehensive presentation of the climate of the basin.

Arguably, the main climatic concern is the influence of a changing Arctic on geographically remote regions. The influence can occur, for example, through freshwater export potentially weakening the

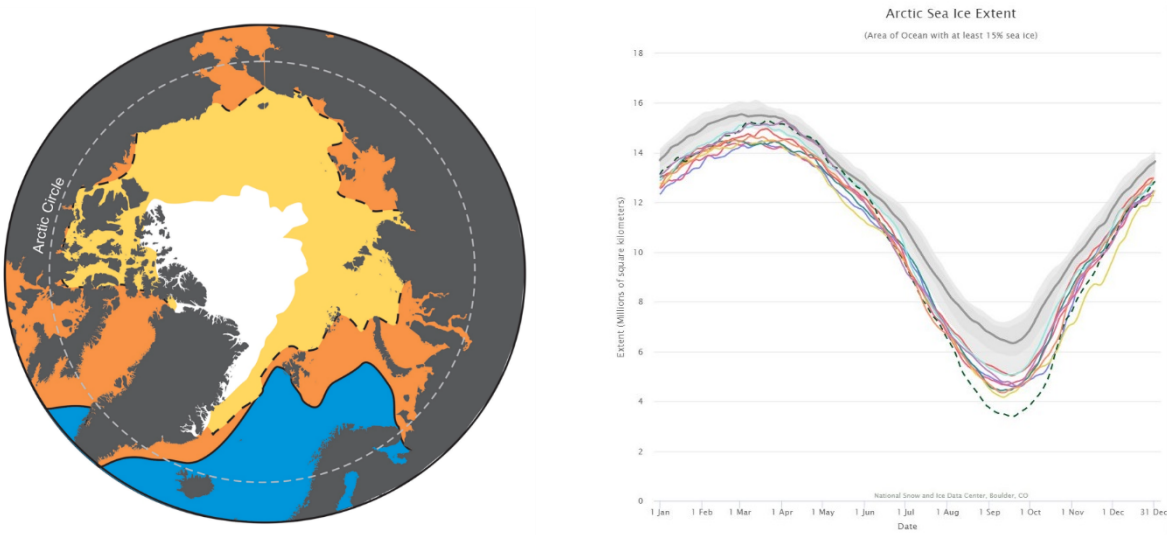

Figure 1.6.1. The Arctic Mediterranean and its changing sea ice cover. The ocean basin and its retreating sea ice cover (left panel; placeholder, source: Malin Daase and Jørgen Berge, UiT). The extent of the yellow and orange regions, respectively, displays the summer minimum and winter maximum sea ice cover of 1980; the white region is the minimum sea ice extent of September 2012. The yellow region thus illustrates the loss in perennial sea ice and translation into a seasonal ice cover over the period. The right panel (needs slight revision wrt, e.g., font size) displays the seasonal cycle of Northern Hemisphere sea ice extent for the years 1980-2018. Black solid line shows 1980-2010 mean seasonal cycle, and the grey shading the interquartile and interdecile range. Colors show individual years since 2010, with 2012 as the dashed line. Sea ice extent is the areas with above 15% ice concentration. Note that some smaller seas outside the Arctic Mediterranean is included in the time series; The Sea of Okhotsk, the Bering Sea, and Hudson and Baffin Bay. (Source nsidc.org/arcticseaicenews/charctic-interactive-sea-ice-graph/)

AMOC (Curry and Mauritzen 2005), and by atmospheric teleconnections perturbing northern hemisphere continental climate from a retreating Arctic sea ice cover (Francis and Vavrus 2015). These matters have large-scale implications and are the topic of much ongoing scientific debate with respect to detection, as well as cause and effect (e.g., Glessmer et al. 2014; Overland et al. 2015). What is well established at present is that the Arctic Mediterranean – and Arctic climate in general – is at the "receiving end" of remote change via ocean circulation, atmospheric teleconnection and global warming (Chapman and Walsh 1993; Eldevik et al. 2014; Årthun et al. 2017; Polyakov et al. 2017; cf. Chapter 10).

1.6.1 Geographical and climatological context

The Arctic Mediterranean's main gateway to the global ocean beyond is the Greenland-Scotland Ridge connecting it with the North Atlantic Ocean (Fig. 1.6.1). About 9 Sv of warm and saline Atlantic Water flows north, mainly between Iceland and Scotland, and cold water returns to the Atlantic proper. Flowing south are the dense Overflow Water (about 6 Sv), at depth through the Denmark Strait and the Faroe-Shetland Channel, and the buoyant low-salinity Polar Water with the East Greenland

Current (2–3 Sv) through the Denmark Strait (Hansen and Østerhus 2000; Østerhus et al. 2018). The overflow water, including entrainment south of the ridge, makes up about ⅔ of North Atlantic Deep Water (Dickson and Browne 1994) that constitutes the deep limb of the Atlantic Meridional Overturning Circulation (AMOC). In addition, there is Pacific inflow through the Bering Strait (about 1 Sv; Woodgate et al. 2010) and a similar outflow through the Canadian Archipelago.

The water mass transformation from Atlantic inflow into overflow and low-salinity outflow is the result of substantial heat loss (about 300 TW) and freshwater input (about 0.2 Sv) in the Arctic Mediterranean (Eldevik and Nilsen 2013). Heat is mainly lost over the Norwegian and Barents seas (Mauritzen 1995) and freshwater is largely provided in the Arctic Ocean (Haine et al. 2015). The heat exchange with the atmosphere is however strongly modified by the large seasonal cycle of the sea ice cover, including net warming of the ocean during summer and a seasonal surface mixed-layer. The freshwater forcing is greatly enhanced by the large surrounding continents where precipitation runs off into major rivers draining into the shallow Arctic shelf seas.

The Arctic Mediterranean is accordingly separated qualitatively – and very broadly – into three water mass domains (the reader is referred to, e.g., Aagaard et al. 1985, and Blindheim and Rey 2004, for a more detailed account of water masses). The warm and saline Atlantic domain extends with the Gulf Stream's northern limb at the eastern side of the basin, in the Norwegian Sea, into the Barents Sea and toward – and with climate change increasingly through – the Fram Strait. The Polar domain of surface low-salinity water covers the upper Arctic Ocean and is exported with the East Greenland Current, concurrent with the extent of the seasonal (winter maximum) sea ice cover. What remains, the bulk of water that fills the Arctic Mediterranean, can broadly be described as Atlantic-derived water that has given up its heat and thus densified to reside below these two more buoyant domains. (It extends all the way to the surface in the central Greenland and Iceland seas). The dense overflow water spilling across the Greenland-Scotland Ridge feeds from this so-called Arctic domain (Aagaard et al. 1985).

The arrival of the sun in spring dictates the Arctic seasonal cycle. At the peak of summer in late June over 300 W/m² reaches the Arctic Ocean in the daily mean (Björk and Söderkvist, 2002), gradually decreasing until Polar night with zero solar radiation from November onwards. The spring sun first melts the snow, both on land and on sea ice, and ends further sea ice growth as the net ocean-atmosphere heat flux starts to warm the surface. Maximum Northern Hemisphere sea ice cover therefore occurs in March in the spatial mean. (Fig 1.6.1). The local sea ice maximum naturally varies with latitude in different regions (Zwally and Gloersen, 2008), as the melting starts earlier in the south. The maximum rate of ice loss occurs at the peak of summer solar radiation in June (Fig. 1.6.1).

The solar forcing during summer warms the ocean mixed layer, and there is a strong positive feedback towards more local melt once the sea ice cover has started to become fractured and significant portions of open water appear. As long as the ice is melting surface temperatures remain close to the freezing point of water, and the largest warming is consistently found in October and November (Overland et al. 2008). Along with the summer surface layer warming there is also a freshening from local sea ice melt and the river inflow that peaks in early summer from the melted land snow (Björk and Söderkvist, 2002). The warming and the freshening remain close to the surface as buoyancy is added. In the Barents Sea the surface warming and freshening goes down to about 50 m (Smedsrud et al. 2010) and can vary with local wind mixing. There is also a seasonal cycle deeper down in the

Arctic Basin, stemming from the Atlantic Water inflow peak in summer heating that slowly circumvents the basin cyclonically (Lique and Steel 2012).

1.6.2 Interannual variability and beyond

The general large-scale horizontal circulation of the Arctic Mediterranean is cyclonic – in general and within individual basins. The cyclonic circulation is sustained by the climatological winds and bottom topography (Nøst and Isachsen 2003; Furevik and Nilsen 2005). Interannual variability in the exchanges with the Pacific and Atlantic oceans through the Bering Strait and across the Greenland-Scotland Ridge, respectively, can also largely be related to wind forcing (Woodgate et al. 2005; Bringedal et al. 2018). However, buoyancy forcing is understood to be increasingly important for longer time scales (Spall 2011; Bringedal et al. 2018).

A general loss of sea ice has been observed since the 1980's in the Northern Hemisphere (Fig. 1.6.1). In the annual mean this amounts to about 2.5 mill km², an area 5 times that of France. There is a clear seasonal contrast in the ice loss with larger loss during summer (September, about 3 mill km² lost) compared to winter (March, about 2 mill km² lost). This seasonal contrast increases if only the Arctic shelf seas are considered, because the Arctic Basin still effectively freezes over in winter (Onarheim et al. 2018).

Since 2010 all years have generally had lower sea ice extent throughout the year than the interdecadal range for 1980-2010. The minimum sea ice extent in the record still corresponds to 2012 (Fig. 1.6.1). The Arctic summer sea ice loss is thus not monotonic or even linear, indicating that natural climate variability is present in the Arctic climate for ice loss (Swart et al. 2015) and also in general (see a more detailed discussion in Chapter 10). Smedsrud et al (2013) demonstrated that multi-decadal variability has been present in the Barents Sea over the last 2500 years, and Årthun et al (2019) showed that for the next few decades an increase in sea ice cover in the Barents Sea is quite likely.

There are a number of negative feedbacks in the Arctic climate system that contribute to preventing "tipping-point-behaviour" and help explain the somewhat surprising linear relationship between the global atmospheric CO2 concentration and Arctic sea ice extent (Notz and Stroeve, 2016). One of these relate to teleconnections and the net freshwater input to the Arctic Ocean that is expected to increase in the future (Bintanja et al., 2018). The increased freshwater input will lead to an increased stratification, and to better protect the Arctic sea ice from the available heat in the warm Atlantic layer (Nummelin et al., 2016). Other negative feedbacks for the sea ice are related to snow cover. This may get thinner because the autumn snow falls into open ocean with the smaller sea ice cover, this will help grow more sea ice because snow effectively insulates the sea ice from the colder atmosphere. A third negative feedback is the sea ice cover itself; when it gets thinner it grows more effectively and ridges more effectively. Wind forcing is generally stronger in the Nordic Seas during winter when there is also a larger temperature gradient between the Arctic and sub-polar seas. Changes in atmospheric circulation may have occurred in relation to the sea ice loss but a longer record is needed to obtain significant conclusions on this relationship.

1.6.3 Global warming and Arctic Amplification

Presently global surface warming over land and sea is 0.87°C above the 1850–1900 mean (IPCC, 2013). Observations in the Arctic are generally not available this far back in time, but the Arctic surface has

clearly warmed more than the global average for the last few decades; this effect is termed 'Arctic Amplification' (Fig. 10.6). Artic amplification is a robust feature in future projections by global models showing a close to twice as large warming for 2100 in the Arctic compared to the global mean (Overland et al., 2018). Thus, the Arctic may warm about 4°C compared to the global 2°C under RCP2.6 or about 10°C compared to the global 5°C under RCP8.5 in the annual mean. Presently, the largest amplitude of amplification is in the Barents Sea (Fig. 10.6) where the largest winter ice loss has occurred (Onarheim et al. 2018). A plausible teleconnection hypothesis is thus that low heat transport from the Atlantic Ocean in the 1980's, and an increase in ocean heat transport since then, has helped drive the Arctic amplification from zero to above four during the last 35 years.

1.7 Ocean Observational Systems

1.7.1 The Global Ocean Observing System

The International Geophysical Year (IGY) from July 1957 to December 1958 may be regarded as the beginning of an era in which systematic studies of the earth and its planetary environment are organized in a framework of international cooperation. The World Ocean, as one of the earth's most ubiquitous environments, was the focus of a large fraction of the IGY studies (Gordon and Baker 1969). The international collaboration in oceanography that started during the IGY evolved considerably in the following decades. By the end of the 1980's, a step further was demanded by the increasing awareness of a possible climate change due to global warming; the need for improved weather and climate forecasts; and the necessity of better knowledge of the impacts of changes in the ocean on the environment, in general. This need for a better coordination and for a continuous and long-term system for ocean observations was clearly formulated during the Second World Climate Conference in Geneva (1990). Following suit, in March 1991, the Global Ocean Observing System (GOOS) was established by the Intergovernmental Oceanographic Commission (IOC).

A crucial component of GOOS consists different programs that deploy and maintain a worldwide array of observing platforms, such as satellites, aircrafts, moored buoys, floats, surface and subsurface drifters, ships of opportunity, remotely operated vehicles and autonomous underwater vehicles. Fig. 1.7.1 shows the in-situ observation implemented under GOOS as of January 2019. Among these, some of the most important observational programs are the moored arrays in the tropical regions of the ocean, the Argo drifting float program and the system represented by the integrated network of satellite-based ocean monitoring system. These three components will be described in more detail in the following sections of this chapter.

To coordinate the enhancement and long-term maintenance of the GOOS integrated global marine meteorological and oceanographic observing and data management system, in 1999 the Joint Technical Commission for Oceanography and Marine Meteorology (JCOMM) was created as a WMO-IOC partnership. As stated in its homepage, JCOMM "is an intergovernmental body of technical experts that provides a mechanism for international coordination of oceanographic and marine meteorological observing, data management and services, combining the expertise, technologies and capacity building capabilities of the meteorological and oceanographic communities".

The creation of this Joint Technical Commission results from a general recognition that worldwide improvements in coordination and efficiency may be achieved by combining the expertise and technological capabilities of WMO and UNESCO's IOC. Under the JCOMM umbrella, the international marine meteorological and oceanographic communities work together to respond to interdisciplinary requirements for observations, data management and service products. All data collected by GOOS and other observational programs are freely available at the JCOMM webpage. It is also possible to know the present status of the Global Ocean Observing system.

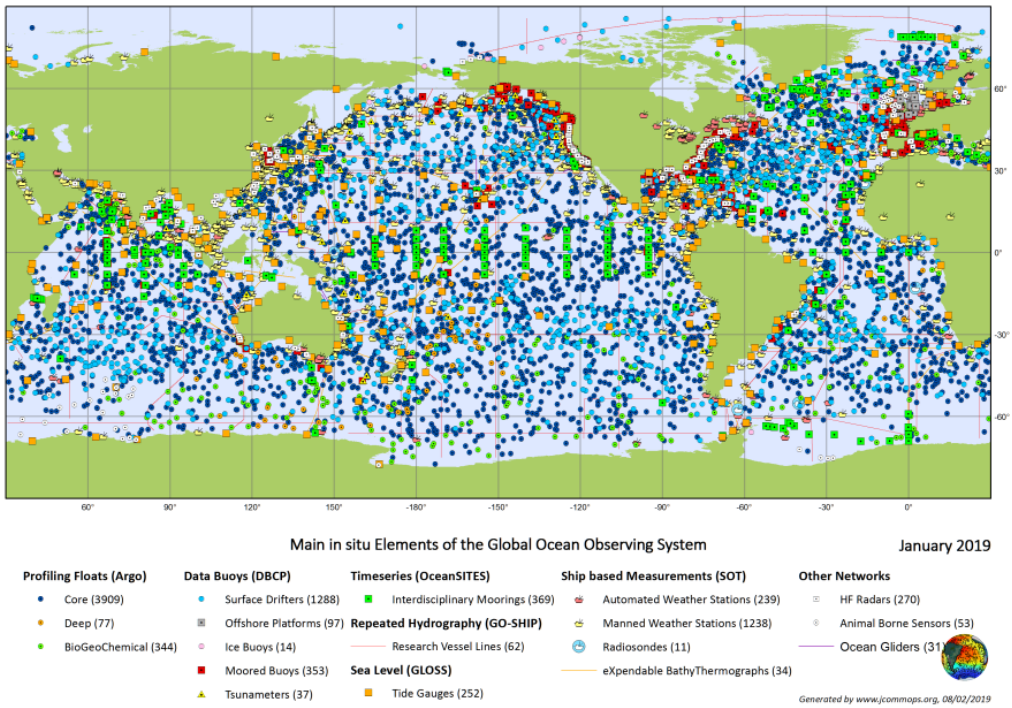

Figure 1.7.1: In-situ instrumentation implemented under GOOS as of January 2019. Maritime zones. SOURCE: http://www.jcommops.org/.

1.7.2 Observing System in the Tropical Oceans

One of the most important components of GOOS is the observational array of moored buoys in the Tropical Oceans. A brief history of this observational platform is presented here.

The TOGA Program. The 1982/1983 El Niño event was one of the most energetic and devastating El Niños ever recorded. This unexpected and unpredicted event was associated with droughts, flooding and a series of other natural disasters all around the globe. The 1982/83 event can be considered a landmark in the history of public awareness of remote climate connections and of the need for a sustained global observation system to monitor and forecast coupled ocean-atmosphere interactions in the tropics.

Efforts towards a better understanding of coupled ocean-atmosphere phenomena existed prior to the 1982-1983 ENSO event. Some of these efforts were the Equatorial Pacific Ocean Climate Studies (EPOCS) program (Hayes et al., 1986), the North Pacific Experiment (NORPAX) (Wyrtki et al., 1981) and

the Pacific Equatorial Ocean Dynamics (PEQUOD) experiment (Eriksen, 1987). The special 1982-1983 event stimulated a concentrated international effort under the auspices of the World Climate Research Program (WCRP). In 1985, the Tropical Ocean Global Atmosphere (TOGA) was started as a 10-year program aiming at the understanding and the prediction of climate events in the time-scale ranging from months to a few years (McPhaden et al., 2010).

TOGA can be regarded as the beginning of the international effort to monitor and deliver in real-time a set of atmospheric and ocean variables essential to improving the capability to predict El Niño and the Southern Oscillation. With this purpose, the deployment of an array of moored buoys was started in the equatorial Pacific. Originally, the moored buoys along this Tropical Atmosphere-Ocean (TAO) array were the low-cost arrangement of a set of monitoring sensors named ATLAS (Autonomous Temperature Line Acquisition System), by NOAA's Pacific Marine Environmental Laboratory (PMEL) (Hayes et al., 1991; McPhaden et al., 1998). Another important component of the TOGA data acquisition system was low-cost drifting (LCD) buoys (Niiler et al., 1995), which provided an accurate way to estimate real-time surface currents.

The TAO/TRITON, PIRATA and RAMA Programs. In the late 1990s and early 2000s the original TAO array was enhanced in the western Pacific, with the addition of the TRITON buoys, and extended to the Tropical Atlantic and Indian Ocean, with the establishment of the PIRATA and RAMA arrays, respectively.

The TRITON buoys (Triangle Trans-Ocean Buoy Network) were introduced In the early 2000s and deployed in the Western Pacific by the Japan Agency for Marine-Earth Science and Technology (JAMSTEC) (Ando et al. 2017). The resulting combined array was referred to, from that time on, as the TAO/TRITON Array. The TRITON buoys are provided and maintained by the Japanese partner, in close cooperation with the NOOA/PMEL, to ensure the necessary consistency with the data sampled by the TAO's ATLAS buoys.

The buoy array in the Tropical Atlantic started as the Pilot Moored Array in the Tropical Atlantic (PIRATA), in 1998, as multinational cooperation between institutions in Brazil, France and the United States. In 2008, after having demonstrated its value and the continued support of the participating institutions, PIRATA became a long-term program, with its name changed to Prediction and Research Moored Array in the Tropical Atlantic (Bourles et al., 2008). In the following years, the observational system in the Tropical Atlantic was significantly enhanced with the deployment of a wide array of observing platforms, including subsurface tall moorings, repeated XBT and glider lines and island-based stations for monitoring meteorological variables and tides, as show in Fig. 1.7.2. A recent contribution was the deployment of a deep mooring to monitor the flux of the Antarctic Bottom Water (AABW) through the Vema Channel.

In 2004, a similar array was started in the Indian Ocean, by means of the Research Moored Array for African-Asian-Australian Monsoon Analysis and Prediction (RAMA), to investigate the role of the ocean in the India Monsoon system, and also to contribute with the understanding of other important climate related processes, such as the IOD (McPhaden et al, 2009). As much as in the Pacific and Atlantic, the RAMA is a multinational effort, involving institutions from India, Japan, China, Australia, Indonesia, France and the United States of America. The buoys in these arrays are currently configured to measure a variety of marine meteorological variables such as winds, air temperature, relative humidity, air pressure, surface radiation, and precipitation; plus sea surface temperature and

salinity, upper ocean temperature and salinity (500-750 m), ocean currents and other parameters. Most of the buoy data are transmitted to shore in real-time for incorporation into operational forecasts and analyses.

1.7.3 The Argo Program

Prior to the year 2000, the knowledge of the ocean thermohaline structure was restricted to vertical

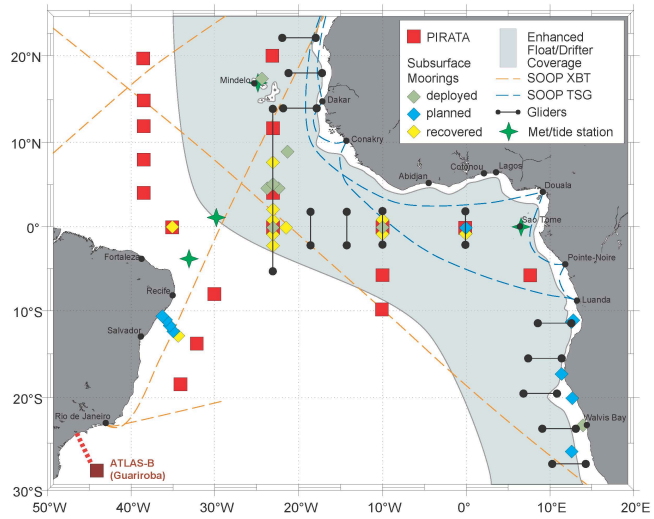

Figure 1.7.2: (.....need figure caption here....)

profiles in points sparsely distributed, both in space and time. There were regions with much less coverage than others and there were many fewer data collected during winter, as compared with the summer seasons. The inadequate coverage was one of the major motivations for the World Ocean Circulation Experiment (WOCE), which is so far the largest international effort aimed to investigate the ocean by means of in situ observations. During its field program, from 1990 to 1998, WOCE gathered an immense dataset, which is freely available and still used in support of research. The information gathered, however, was not enough. Ship-based data collection is very expensive and produces information on very limited areas and in short periods of time. Monitoring based on moored buoys is very helpful in areas where these are deployed. In spite of its considerable magnitude, the WOCE data set was still insufficient to provide the reliable and necessary information to understand the ocean thermohaline structure, its circulation and the role on climate. To ameliorate that, as of the end of the 1990's, the international oceanographic community started to deploy the Argo floats, a newly developed instrument for sampling physical properties in the ocean. This started a completely new era in the study of the oceans.

The Argo floats, named after the mythical ship used by Jason in his quest for the golden fleece, are autonomous profiling devices, programmed to sink and park at a certain depth, where they drift with the local currents. After a predetermined length of time, each float comes back to the surface, sampling water properties during its ascension. At the surface, it transmits via satellite all the information stored in its solid-state memory, which includes its location and the vertical distribution of properties sampled in the water column. Then, according to the way it is programmed, it sinks again, repeating the cycle over and over again, with lifetimes of up to 4-5 years.

The first floats were launched in the year 2000 and as of 27 December 2018, 3945 floats were active in the global ocean. Each year, this array of almost four thousand floats provides over 100,000 vertical profiles of temperature and salinity and an estimate of the velocity at the float's parking depth, distributed on an average 3-degree spacing grid over the entire ocean. Originally, the Argo floats were capable to operate only to 2000m depth and to sample only physical properties (T, S and pressure). More recently, deep Argo floats are being launched with full depth capacity and biogeochemical Argo floats are being deployed with sensors for a variety of chemical and biological variables. All data collected are publicly available in near-real time, after an automated quality control, and in a scientifically-controlled form within one year after collection.

1.7.4 Satellite Observations

To support the work of the United Nations Framework Convention on Climate Change (UNFCC) and the International Panel on Climate Change (IPCC), a number of Essential Climate Variables (ECVs) were defined by the Global Climate Observing System (GCOS). The complete list of ECVs includes over 40 variables for the atmospheric, terrestrial and oceanic components of the climate system. In the Ocean, there are surface and sub-surface essential variables. While the ship-based observations, moored and floating buoys are crucial to sample variables in the water column, it is practically impossible to sample all ocean surface ECVs with the needed spatial and temporal coverage by means of only in situ observations. The measurement of surface variables has been greatly enhanced by satellite remote sensing. Starting in the 1970s, ocean data from satellites have become an essential tool for oceanography. For example, analyses of infrared imagery revealed the existence of tropical instability waves in the Tropical Pacific (Legeckis, 1977).

In general, there are two types of satellites used to observe ocean variables: geostationary and polar-orbiting. Geostationary satellites stay over the same location and, in this way, can document evolving systems. They sample variables over a relatively large area, with high temporal resolution, with no polar coverage. Polar-orbiting satellites travel at relatively lower altitudes, approximately 850 to 1000km, and orbit nearly over the poles. In spite of spending a limited time over each point (i.e. the orbital plane remains nearly constant while the planet rotates).

Nowadays, a vast array of geostationary and polar-orbiting satellites equipped with different sensors is in operation, providing accurate measurements of practically all ECVs at the ocean's surface. The combination of the satellite-based data with in situ observations and numerical models allows for a coherent global mapping of physical variables such as sea surface temperature, salinity, ocean surface topography, winds, currents, sea-ice and waves, as well as biochemical properties such as chlorophyll concentration and phytoplankton content.

1.7.5 Contribution to Climate Forecasting

During the past decades, climate forecast models have greatly benefited from the tropical moored arrays, Argo and satellite data. With the inclusion of this new information, the ability to predict events such as El Niño and other global and regional climate events has significantly improved. Together with faster and more efficient computers, better knowledge of the present conditions contributes to a higher skill of predictions by numerical models.

As an example of the change in perspective, until recently, the two strongest El Niño events ever recorded were those of 1982/83 and 1997/98, each of which could be regarded, at the time of their occurrence, as rare events with a return period of about one hundred years. Afterwards, the 2015/16 El Niño struck with a similar intensity to the previous two major events (L'heureux et al., 2017), setting new records for SST anomalies in the central and western regions of the Equatorial Pacific and impacting living conditions of several million people, particularly in the poorest and most vulnerable regions of the planet. However, the 2015/16 El Niño did not cause the same degree of worldwide disaster as happened in 1997/98. This could be explained to some extent by intrinsic differences between events (e.g., the 2015/16 El Niño had a more muted impact on western South America; Paek et al. 2017). However, the advance knowledge of event occurrence by several months facilitated timely and effective preventive actions by governments and international institutions such as the World Health Organization.

1.8. Synthesis

A more comprehensive understanding of global oceans and their circulation has been obtained by the research community during the past few decades, and this understanding has advanced very rapidly in recent years with the help of more sophisticated observation techniques. These advances have enabled the research communities to explore new directions that were either not easily accessible in the past or had not received much attention until recently. In particular, more information is available to investigate interbasin interaction and associated mechanisms, and their possible variation in time as the background basin circulation also changes. The following highlights the interbasin connections and trends mentioned in this Chapter, which have been reviewed in Cai et al. (2019) and will be examined in more detail in the following chapters.

1.8.1. Pacific Ocean

El Niño induces warming in the tropical Indian Ocean and the tropical North Atlantic Ocean about 3-6 months after the El Niño peaks. Atmospheric wave trains excited by El Niño set up teleconnections that influence remote climates worldwide. The details of such influence can be different between the Eastern Pacific and Central Pacific types of El Niño. The Pacific Meridional Mode can modulate the occurrence of western Pacific typhoon and eastern Pacific hurricane and precipitation patterns in East Asia and South America.

Significant changes occurred in the Pacific and other basins around the time when the Pacific Decadal Oscillation shifted from a negative to a positive phase around 1976–77 and back to a negative phase around 1999–2000.

1.8.2 Atlantic Ocean

The Atlantic Niño impacts the tropical Indian and Pacific Ocean basins. it has been linked to SST anomalies of opposite sign in the subtropical southwestern Atlantic. The Atlantic Niño has direct impacts on the West African Monsoon system. The positive phase is associated with a southward migration of the ITCZ, delaying the monsoon onset. It has been shown that the Atlantic Niño can alter the atmospheric circulation of the North Atlantic-European region in summer, the tropical Indian and Pacific Ocean basins.

The Atlantic Multidecadal Variability has been related to modulation of rainfall in the Sahel and South America, as well as to changes in the extratropical climate.

The Atlantic Meridional Overturning Circulation is a key mechanism for the global redistribution and transport of heat from the Southern to the Northern Hemisphere in the Atlantic. Its variations impact climate variability at different timescales, being a main driver of the Atlantic Multidecadal Variability and a key factor for the redistribution of anthropogenic influences on temperature to the deep ocean.

1.8.3 The Indian Ocean

The strength and frequency of the Indian Ocean Basin Mode are highly related to ENSO. The mode has significant influences on Indo-Pacific Climate through modulations of the monsoon north of the equator and atmospheric circulations over the Northwest Pacific in what is known as the Indian Ocean-Pacific Ocean Capacitor effect. The impacts of the Indian Ocean Basin Mode on the Northwest Pacific climate vary with time, being weaker before 1976/77 and stronger afterwards. Another important basin mode, the Indian Ocean Dipole has remarkable climatic impacts in regional and even global scales, such as heavy rainfall and extensive flooding in equatorial East Africa, drought and bushfire in Indonesia and Australia, and Asian Monsoon intensity. The mode variability can also feedback on ENSO through atmospheric bridges and oceanic pathways.

The Indonesian Throughflow provides the only low-latitude pathway for the transfer of warm and low salinity seawater from the Pacific into the Indian Ocean. Links have been suggested between interdecadal variability of the Indian Ocean Dipole and the Indonesian Throughflow.

1.8.4 The Southern Ocean

Rapid ice shelf melt around Antarctica has the potential to accelerate the motion of ice sheets, resulting in a reduction in total land ice and correspondingly higher global sea level. SAM and ENSO can influence the winds around Antarctica, with ENSO effects particularly evident in the Pacific sector. El Niño events are associated with warming and increased ice melt in the region of the Antarctic Peninsula.

The Southern Ocean has warmed and freshened over the last 50 to 100 years, and Argo measurements points to it as the region of the world's ocean that is undergoing the most rapid increase in ocean heat content, possibly due to increased greenhouse gases with some contribution from ozone depletion.

1.8.5 The Arctic Mediterranean

A changing climate in the Arctic basin can affect geographically remote regions. The Arctic surface has warmed more than the global average for the last few decades defining the 'Arctic Amplification' which is a robust feature in future projections by global models. Increased melting and freshwater export can potentially weaken the Atlantic Meridional Overturning Circulation. Moreover, retreating Arctic sea ice cover can trigger atmospheric teleconnections that perturb continental climates, especially in the Northern Hemisphere. Lower heat transport from the Atlantic Ocean in the 1980's, and an increase since then has helped drive the Arctic amplification from zero to above four during the last 35 years. Teleconnections and net freshwater input to the Arctic Ocean, which is expected to increase in the future, may contribute to preventing "tipping-point-behaviour" of the Arctic climate.

The Arctic Mediterranean is directly connected with the Pacific and Atlantic Oceans through the Bering Strait and across the Greenland-Scotland Ridge, respectively.

Acknowledgments

J.-Y. Yu was supported by the National Science Foundation under grants AGS1505145 and AGS-1833075. STG was supported by the National Science Foundation under grants OCE-1658001 and PLR-1425989.……

References

Aagaard, K., Swift, J. H., and Carmack, E. C. (1985). Thermohaline circulation in the Arctic Mediterranean Seas, *J. Geophys. Res*., **90**(C3), 4833–4846.

Abernathey, R., J., Mazloff, M., and Shuckburgh, E. (2010). Enhancement of Mesoscale Eddy Stirring at Steering Levels in the Southern Ocean. *J. Phys. Oceanogr*., **40**, 170–184.

Alexander, M. A., and Deser, C. (1995). A mechanism for the recurrence of wintertime midlatitude SST anomalies. *J. Phys. Oceanogr*., **25**, 122–137.

Alexander, M. A., Blade, I., Newman, M., Lanzante, J. R., Lau, N.-C., and Scott, J. D. (2002). The atmospheric bridge: The influence of ENSO teleconnections on air-sea interaction over the global oceans*, J. Climate*, **15**, 2205–2231.

Alexander, M. A., Vimont, D. J., Chang, P., and Scott, J. D. (2010). The impact of extratropical atmospheric variability on ENSO: Testing the seasonal footprinting mechanism using coupled model experiments. *J. Climate*, **23**, 2885-2901.

Alexander, M. A., Kilbourne, K. H., and Nye, J. A. (2014). Climate variability during warm and cold phases of the Atlantic Multidecadal Oscillation (AMO) 1871–2008. *Journal of Marine Systems*, **133**, 14-26.

Amaya, D. J., Bond, N. E., Miller, A. J., and DeFlorio, M. J. (2016). The evolution and known atmospheric forcing mechanisms behind the 2013-2015 North Pacific warm anomalies. *US CLIVAR Variations*, **14**(2), US CLIVAR, Washington, DC, 1–6, https://usclivar.org/newsletter/newsletters.

Amaya, D. J., DeFlorio, M. J., Miller, A. J., and Xie, S. P. (2017). WES feedback and the Atlantic Meridional Mode: observations and CMIP5 comparisons. *Clim. Dyn.*, **49**(5-6), 1665-1679.

An, S-I (2004). A dynamical linkage between the monopole and dipole modes in the tropical Indian Ocean. *Theor Appl Climatol*, **78**, 195–201.

Anderson, B. T. (2004). Investigation of a large-scale mode of ocean atmosphere variability and its relation to tropical Pacific sea surface temperature anomalies. *J. Climate*, **17**, 1089–4098.

Ando, K., Kuroda, Y., Yosuke, F. Fukuda, T., Hasegawa, T., Horii, T., Ishihara, Y., Kashino, Y., Masumoto, Y., Mizuno, K., Nagura, M., and Ueki, I. (2017). Fifteen years progress of the TRITON array in the Western Pacific and Eastern Indian Oceans*. J. Oceanography*. **73**(4), 403-426.

Annamalai, H., Murtugudde, R., Potemra, J., et al. (2003), Coupled dynamics over the Indian Ocean: spring initiation of the Zonal Mode, *Deep Sea Research Part II: Topical Studies in Oceanography*, **50**, 2305-2330.

Annamalai, H., Xie, S. P., McCreary, J. P., et al. (2005), Impact of Indian Ocean sea surface temperature on developing El Niño, *J. Climate*, **18**, 302-319.

Aoki, S., Rintoul, S. R., Ushio, S., Watanabe, S., and Bindoff, N. L. (2005). Freshening of the Adelie Land Bottom Water near 140°E. *Geophys. Res. Lett.*, **32**, L23601.

Armour, K.C., Marshall, J., Scott, J. R., Donohoe, A., and Newsom, E. R. (2016). Southern Ocean warming delayed by circumpolar upwelling and equatorward transport, *Nature Geoscience*, **9**, 549–554.

Årthun, M, Eldevik, T. and Smedsrud, L.H. (2019). The role of Atlantic heat transport in future Arctic winter sea ice variability and predictability, *J. Climate*, In Press.

Årthun, M., Eldevik, T., Viste, E., Drange, H., Furevik, T., Johnson, H. L., and Keenlyside, N. S. (2017). Skillful prediction of northern climate provided by the ocean. *Nature Communications*, **8**.

Ashok, K., Chan, W. L., Motoi, T., et al. (2004). Decadal variability of the Indian Ocean dipole, *Geophys. Res. Lett*., **31**, L24207.

Ashok, K., Behera, S. K., Rao, S. A., Weng, H., and Yamagata, T. (2007). El Niño Modoki and its possible teleconnection. *J. Geophy. Res*., **112**, C11007.

Baldwin, M. P. and Dunkerton, T. J. (2001). Stratospheric harbingers of anomalous weather regimes, *Science*, **244**, 581–584.

Behera, S. K., Krishnan, R., and Yamagata, T. (1999). Unusual ocean-atmosphere conditions in the tropical Indian Ocean during 1994, *Geophys. Res. Lett*., **26**, 3001–3004

Behera, S. K., and Yamagata, T. (2003). Influence of the Indian Ocean Dipole on the southern oscillation, *J. Meteorol. Soc. Japan*., **81**, 169-177

Bintanja, R., Katsman, C. A., and Selten, F. M. (2018). Increased Arctic precipitation slows down sea ice melt and surface warming. *Oceanography*, **31**(2), 119-125.

Bjerknes, J. (1969). Atmospheric teleconnections from the equatorial Pacific. *Monthly Weather Review*, *97*(3), 163-172.

Björk, G., and Söderkvist, J. (2002). Dependence of the Arctic Ocean ice thickness distribution on the poleward energy flux in the atmosphere, *J. Geophys. Res*., **107**(C10), 3173.

Blindheim, J., and Rey, F., (2004). Water-mass formation and distribution in the Nordic Seas during the 1990s. *ICES Journal of Marine Science*, **61**, 846–863.

Bond, N. A., Cronin, M. F., Freeland, H., and Mantua, N. (2015). Causes and impacts of the 2014 warm anomaly in the NE Pacific. *Geophys. Res. Lett*., **42**, 3414–3420.

Böning, C., Dispert, A., Visbeck, M., Rintoul, S. R. & Schwarzkopf, F. U. (2008). The response of the Antarctic Circumpolar Current to recent climate change. *Nature Geoscience*, **1**, 864–869.

Bourlès, B., Rick Lumpkin, McPhaden, M. J., Hernandez, F., Nobre, P., Campos, E., Yu, L., Planton, S., Busalacchi, A., Moura, A. D., Servain, S., and Trotte, J. (2008). THE PIRATA PROGRAM: History, Accomplishments, and Future Directions. *Bull. Amer. Meteor. Soc*. 1112-1125.

Bringedal, C., Eldevik, T., Skagseth, Ø., Spall, M., and Østerhus, S. (2018). Structure and forcing of observed exchanges across the Greenland-Scotland Ridge. *J. Climate*, **31**, 9881–9901

Bruce, J. (1973). Equatorial undercurrent in the western Indian Ocean during the southwest monsoon. *J. Geophys. Res*., **78**, 6386-6394.

Buckley, M. W., & Marshall, J. (2016). Observations, inferences, and mechanisms of the Atlantic Meridional Overturning Circulation: A review. Reviews of Geophysics, 54(1), 5-63.

Cai, W. (2006). Antarctic ozone depletion causes an intensification of the Southern Ocean super-gyre circulation. *Geophys. Res. Lett*, **33**. L03712.

Cai, W., Meyers, G., and Shi, G. (2005). Transmission of ENSO signal to the Indian Ocean, *Geophys. Res. Lett.*, **32**, 347-354.

Cai, W. and Cowan, T. (2007). Trends in Southern Hemisphere circulation in IPCC AR4 models over 1950–99: Ozone depletion versus greenhouse forcing*. J. Climate*, **20**, 681–693.

Cai, W., Cowan, T., and Sullivan, A. (2009). Recent unprecedented skewness towards positive Indian Ocean Dipole occurrences and its impact on Australian rainfall, *Geophys. Res. Lett.*, **36**, 245-253.

Cai, W., and Qiu, Y. (2013). An Observation-Based Assessment of Nonlinear Feedback Processes Associated with the Indian Ocean Dipole, *J. Climate*, **26**, 2880-2890.

Cai, W.L. Wu, M. Lengaigne, Tim Li, S. McGregor, J.-S. Kug, J.-Y. Yu, M.F. Stuecker, A. Santoso, X. Li, Y.-G. Ham, Y. Chikamoto, B. Ng, M.J. McPhaden, Y. Du, D. Dommenget, F. Jia, J.B. Kajtar, N. Keenlyside, X. Lin, J.-J. Luo, M. Martín del Rey, Y. Ruprich-Robert, G. Wang, S.-P. Xie, Y. Yang, S.M. Kang, J.-Y. Choi, B. Gan, G.-I. Kim, C.-E. Kim, S. Kim, J.-H. Kim, P. Chang, 2019: Pan-tropical climate interactions. Science, 36(6430), eaav4236.

Capotondi, A., Wittenberg, A. T., Newman, M., Di Lorenzo, E., Yu, J.-Y., et al. (2015). Understanding ENSO diversity. *Bull. Amer. Meteor. Soc*., **96**, *921-938*.

Chang, P., Ji, L., & Li, H. (1997). A decadal climate variation in the tropical Atlantic Ocean from thermodynamic air-sea interactions. *Nature*, **385**(6616), 516.

Chang, P., L. Zhang, R. Saravanan, D. J. Vimont, J. C. H. Chiang, L. Ji, H. Seidel, and M. K. Tippett (2007). Pacific meridional mode and El Niño-Southern Oscillation. *Geophys. Res. Lett*., **34**, L16608.

Chapman, W. L., and Walsh, J. E. (1993). Recent Variations of Sea Ice and Air Temperature in High Latitudes. *Bull. Amer. Meteor. Soc*., **74**, 33–47.

Chen, G., Han, W., Li, Y., Wang, D., and McPhaden, M. J. (2015). Seasonal-to-Interannual Time-Scale Dynamics of the Equatorial Undercurrent in the Indian Ocean*. *J. Phys. Oceanogr.*, **45**(6), 1532–1553.

Chen, G. X., Han, W. Q., Li, Y. L., et al. (2016). Interannual Variability of Equatorial Eastern Indian Ocean Upwelling: Local versus Remote Forcing, *J. Phys. Oceanogr*., **46**, 789-807.

Chen, Z., Wen, Z., Wu, R., Lin, X., and Wang, J. (2016). Relative importance of tropical SST anomalies in maintaining the western north Pacific anomalous anticyclone during El Niño to la Niña transition years. *Clim. Dyn*., **46**, 1027-1041.

Chen, Z., Wen, Z., Wu, R., and Du, Y. (2017). Roles of tropical SST anomalies in modulating the western north pacific anomalous cyclone during strong la Niña decaying years. *Clim. Dyn*., **49**, 633-647.

Chiang, J. C., and Vimont, D. J. (2004). Analogous Pacific and Atlantic meridional modes of tropical atmosphere-ocean variability, *J. Climate*, **17,** 4143-4158.

Ciasto, L. M., and Thompson, D. W. J. (2008). Observations of largescale ocean–atmosphere interaction in the Southern Hemisphere. *J. Climate*, **21**, 1244–1259.

Clement, A., Bellomo, K., Murphy, L. N., Cane, M. A., Mauritsen, T., Rädel, G., & Stevens, B. (2015). The Atlantic Multidecadal Oscillation without a role for ocean circulation. *Science*, **350**(6258), 320-324

Comiso, J. C. (2010). Variability and trends of the global sea ice cover, in: Sea Ice, 2nd edn., Wiley-Blackwell, Oxford, UK, 205–246.

Comiso, J. C. and Nishio, F. (2008). Trends in the sea ice cover using enhanced and compatible AMSR-E, SSM/I, and SMMR data, *J. Geophys. Res.*, **113**, C02S07.

Conway, D. (2002). Extreme rainfall events and lake level changes in East Africa: Recent events and historical precedents, *Adv. Glob. Change Res*., **12**, 63-92

Cresswell G R, and Golding, T J. (1980). Observations of a south-flowing current in the southeastern Indian Ocean. *Deep Sea Research Part A. Oceanographic Research Papers*, **27**(6), 449-466.

Curry, R., and Mauritzen, C. (2005). Dilution of the Northern North Atlantic Ocean in recent decades. *Science*, **308**, 1772–1774.

Danabasoglu, G., Yeager, S. G., Kwon, Y. O., Tribbia, J. J., Phillips, A. S., & Hurrell, J. W. (2012). Variability of the Atlantic meridional overturning circulation in CCSM4. *J. Climate*, **25**(15), 5153-5172.

Delman, A. S., Sprintall, J., McClean, J. L., et al. (2016). Anomalous Java cooling at the initiation of positive Indian Ocean Dipole events, *J. Geophys. Res.-Oceans*, **121**, 5805-5824

Deppenmeier, A. L., Haarsma, R. J., & Hazeleger, W. (2016). The Bjerknes feedback in the tropical Atlantic in CMIP5 models. *Clim. Dyn*., **47**(7-8), 2691-2707.

Delworth, T., Manabe, S., and Stouffer, R. J. (1993). Interdecadal variations of the thermohaline circulation in a coupled ocean-atmosphere model. *J. Climate*, **6**(11), 1993-2011.

Delworth, T. L., and Greatbatch, R. J. (2000). Multidecadal thermohaline circulation variability driven by atmospheric surface flux forcing. *J. Climate*, **13**(9), 1481-1495.

Delworth, T. L., and Mann, M. E. (2000). Observed and simulated multidecadal variability in the Northern Hemisphere. *Clim. Dyn*., **16**(9), 661-676

Delworth, T. L., and Zeng, F. (2016). The impact of the North Atlantic Oscillation on climate through its influence on the Atlantic meridional overturning circulation. *J. Climate*, **29**(3), 941-962.

Deser, C., and Blackmon, M. L. (1993). Surface climate variations over the North Atlantic Ocean during winter: 1900–1989. *J. Climate*, **6**(9), 1743-1753.

Dickson, R. R., and Brown, J. (1994). The production of North Atlantic deep water: Sources, rates and pathways. *J. Geophys. Res*., **99**, 12319–12342.

Di Lorenzo, E., and N. Mantua (2016). Multi-year persistence of the 2014/15 North Pacific marine heatwave. *Nat. Climate Change*, **6,** 1042–1047.

Dippe, T., Greatbatch, R. J., & Ding, H. (2017). On the relationship between Atlantic Niño variability and ocean dynamics. *Clim. Dyn*., **51** (1-2), 1-16.

Dieppois, B., et al. (2015). Low-frequency variability and zonal contrast in Sahel rainfall and Atlantic sea surface temperature teleconnections during the last century. *Theoretical and applied climatology*, **121**(1-2), 139-155.

Ding, H., Keenlyside, N. S., & Latif, M. (2012). Impact of the equatorial Atlantic on the El Niño southern oscillation. *Clim. Dyn*., **38**(9-10), 1965-1972.

Ding, Q., Steig, E. J., Battisti, D. S. & Küttell, M. (2011). Winter warming in West Antarctica caused by central tropical Pacific warming. *Nature Geosci*., **4**, 398–403.

Domingues, C. M., Maltrud, M. E., Wijffels, S. E., Church, J. A., and Tomczak, M. (2007). Simulated lagrangian pathways between the leeuwin current system and the upper-ocean circulation of the southeast indian ocean. *Deep-Sea Research Part II*, **54**(8), 797-817.

Donohue, K. A., Tracey, K. L., Watts, D. R., Chidichimo, M. P., and Chereskin, T. K. (2016). Mean Antarctic Circumpolar Current transport measured in Drake Passage, *Geophys. Res. Lett*., **43**, 11,760–11,767.

Du, Y., Xie, S.-P., Huang, G., et al. (2009). Role of air-sea interaction in the long persistence of El Niño-induced North Indian Ocean warming. *J. Climate*, **22**, 2023-2038.

Du, Y., Yang, L., Xie, S.-P. (2011). Tropical Indian Ocean influence on Northwest Pacific tropical cyclones in summer following strong El Niño. *J. Climate*, **24**, 315–322.

Du, Y., Cai, W. J., and Wu, Y. L. (2013). A New Type of the Indian Ocean Dipole since the Mid-1970s, *J. Climate*, **26**, 959-972.

Durack, P. J., Wijffels, S. E. and Matear, R. J. (2012). Ocean salinities reveal strong global water cycle intensification during 1950 to 2000. *Science*, **336**, 455–458.

Eisenman, I., Meier, W. N., and Norris, J. R. (2014). A spurious jump in the satellite record: has Antarctic sea ice expansion been overestimated?, *The Cryosphere*, **8**, 1289-1296.

Eldevik, T. and J.E.Ø. Nilsen (2013). The Arctic–Atlantic thermohaline circulation. *J. Climate*, **26**, 8698–8705.

Eldevik, T., Risebrobakken, B., Bjune, A. E., Andersson, C., Birks, H. J. B., Dokken, T. M., Drange, H., Glessmer, M. S., Li, C., Nilsen, J. E. Ø., Otterå, O. H., Richter, K. and Skagseth, Ø. (2014). A brief history of climate – the northern seas from the Last Glacial Maximum to global warming. *Quat. Sci. Rev.,* **106**, 225–246.

Enfield, D. B., & Mayer, D. A. (1997). Tropical Atlantic sea surface temperature variability and its relation to El Niño-Southern Oscillation. *J. Geophys. Res.-Oceans*, **102**(C1), 929-945.

Enfield, D. B., Mestas-Nuñez, A. M., & Trimble, P. J. (2001). The Atlantic multidecadal oscillation and its relation to rainfall and river flows in the continental US. *Geophys. Res. Lett*., **28**(10), 2077-2080.

England, M. H., McGregor, S., Spence, P., Meehl, G. A., Timmermann, A., Cai, W., Gupta, A. S., McPhaden, M. J., Purich, A., and Santoso, A. (2014). Recent intensification of wind-driven circulation in the Pacific and the ongoing warming hiatus, *Nat. Clim. Change*, **4**, 222–227.

Eriksen, C. (1987). A review of PEQUOD, in Further Progress in Equatorial Oceanography, edited by E. J. Katz and J. M. Witte, pp. 29-46, Nova Univ. Press, Fort Lauderdale, Fla.

Fan, M., and Schneider, E. K. (2012). Observed decadal North Atlantic tripole SST variability. Part I: Weather noise forcing and coupled response. *J. Atmos. Sci*., **69**(1), 35-50.

Feng, M., and Meyers, G. (2003). Interannual variability in the tropical Indian Ocean: a two-year time-scale of Indian Ocean Dipole, *Deep Sea Research Part II: Topical Studies in Oceanography*, **50**, 2263-2284.

Fogt, R. L., and Bromwich, D. H. (2006). Decadal variability of the ENSO teleconnection to the high latitude South Pacific governed by coupling with the Southern Annular Mode. *J. Climate*, **19**, 979–997.

Foltz, G. R., and McPhaden, M. J. (2010). Interaction between the Atlantic meridional and Niño modes. *Geophys. Res. Lett*., **37**, L18604.

Francis, J. A., and Vavrus, S. J. (2015). Evidence for a wavier jet stream in response to rapid Arctic warming. *Env. Res. Lett*., **10**, 014005.

Frierson, D. M., Hwang, Y. T., Fučkar, N. S., Seager, R., Kang, S. M., Donohoe, A., ... & Battisti, D. S. (2013). Contribution of ocean overturning circulation to tropical rainfall peak in the Northern Hemisphere. *Nature Geoscience*, **6**(11), 940-944.

Furue, R., Mccreary, J. P., Benthuysen, J., Phillips, H. E., and Bindoff, N. L. (2013). Dynamics of the leeuwin current: part 1. coastal flows in an inviscid, variable-density, layer model. *Dynamics of Atmospheres and Oceans*, **63**, 24-59.

Fyfe, J. C. & Saenko, O. A. (2006). Simulated changes in the extratropical Southern Hemisphere winds and currents. *Geophys. Res. Lett.,* **33**. L06701.

Ganachaud, A., and Wunsch, C. (2000) Improved estimates of global ocean circulation, heat transport and mixing from hydrographic data, *Nature*, **408**, 453-457.

García-Serrano, J., Losada, T., & Rodríguez-Fonseca, B. (2011). Extratropical atmospheric response to the Atlantic Niño decaying phase. *J. Climate*, **24**(6), 1613-1625.

García-Herrera, R., N. Calvo, R. R. Garcia, and M. A. Giorgetta (2006). Propagation of ENSO temperature signals into the middle atmosphere: A comparison of two general circulation models and ERA-40 reanalysis data, *J. Geophys. Res*., **111**, D06101.

Gentemann, C. L., Fewings, M. R., and García-Reyes, M. (2017). Satellite sea surface temperatures along the West Coast of the United States during the 2014–2016 northeast Pacific marine heat wave. *Geophys. Res. Lett.*, **44**, 312–319.

Gille, S. T. (2002). Warming of the Southern Ocean since the 1950s, *Science*, **295**, 1275-1277.

Gille, S. T. (2008). Decadal-scale temperature trends in the Southern Hemisphere ocean, *J. Climate*, **21**(18), 4749-4765.

Gille, S. T. (2014). Meridional Displacement of the Antarctic Circumpolar Current, *Phil. Trans. Roy. Soc. A.*, **372**, 20130273.

Glessmer, M. S., Eldevik, T., Våge, K., Nilsen, J. E. Ø. and Behrens, E. (2014). Atlantic origin of observed and modelled freshwater anomalies in the Nordic Seas. *Nature Geoscience,* **7**, 801–805.

Goldenberg, S. B., Landsea, C. W., Mestas-Nuñez, A. M., & Gray, W. M. (2001). The recent increase in Atlantic hurricane activity: Causes and implications. *Science*, **293**(5529), 474-479.

Gordon, A. L. and Baker, F. W. G. (1969). Eds. Oceanography. Volume 46 in Annals of the International Geophysical Year. Elsevier Ltd., 226pp.

Gordon A L. (1986). Interocean exchange of thermocline water. *J. Geophys. Res.-Oceans*, **91**(C4), 5037-5046.

Gordon A L. (2005). The indonesian seas. *Oceanography*, **18**(4), 14.

Griesel, A., Gille, S. T., Sprintall, J., McClean, J. L., LaCasce, J. H., and Maltrud, M. E. (2010). Isopycnal diffusivities in the Antarctic Circumpolar Current inferred from Lagrangian floats in an eddying model, *J. Geophys. Res.*, **115**, C06006.

Gu, D., and Philander, S> G. H. (1997). Interdecadal climate fluctuations that depend on exchanges between the tropics and extratropics. *Science*, **275**, 805–807.

Guan, Z. Y., and Yamagata, T. (2003), The unusual summer of 1994 in East Asia: IOD teleconnections, *Geophys. Res. Lett.*, **30**, 1544.

Haarsma, R. J., and Hazeleger, W. (2007). Extratropical atmospheric response to equatorial Atlantic cold tongue anomalies. *J. Climate*, **20**(10), 2076-2091

Haine, T. W. N., et al. (2015), Arctic freshwater export: Status, mechanisms, and prospects, *Glob-al Planet. Change*, **125**, 13–35.

Han, W., Vialard, J., McPhaden, M. J., Lee, T., Masomoto, Y., Feng, M., and de Ruijter, W. (2014). Indian Ocean decadal variability: a review. Bull. Amer. Meteor. Soc..

Hansen, B., and Østerhus, S. (2000). North Atlantic–Nordic Seas exchanges. *Prog. Oceanogr.*, **45**, 109–208.

Hartmann, D. L. (2015). Pacific sea surface temperature and the winter of 2014. *Geophys. Res. Lett.*, **42**, 1894–1902.

Hayes, S. P. et al. (1986). The Equatorial Pacific Ocean Climate Studies (EPOCS) Plans: 1986-1988, *EOS rans*. AGU, **67**, 442-444.

Hayes, S.P., Mangum, L. J., Picaut, J., Sumi, A., and Takeuchi, K. (1991). TOTA TAO: A moored Array for real-time measurements in the tropical Pacific Ocean. *Bull. Am. Meteorol. Soc*. **72**, 339-347.

Haumann F. A., Gruber, N. Münnich, M., Frenger, I., and Kern, S. (2016). Sea ice transport driving Southern Ocean salinity and its recent trends. *Nature*, **537**, 89–92.

Hellerman S, and Rosenstein M. (1983). Normal monthly wind stress over the world ocean with error estimates. *J. Physical* Oceanogr, **13**(7), 1093-1104.

Hirst, A. C., and Godfrey, J. (1993). The role of Indonesian throughflow in a global ocean GCM. *J. Phys. Oceanogr.*, **2**3, 1057–1086.

Hu K. M., Huang G., and Huang R. H. (2011). The impact of tropical Indian Ocean variability on summer surface air temperature in China. *J. Climate*, **24**, 5365–5377.

Hu K. M., Huang G., and Wu R. (2013). A strengthened influence of ENSO on August high temperature extremes over the southern Yangtze River valley since the late 1980s. *J. Climate*, **26**, 2205–2221.

Hu, Z.-Z., Kumar, A., Jha, B., Zhu, J., and Huang, B. (2017). Persistence and predictions of the remarkable warm anomaly in the northeastern Pacific Ocean during 2014–16. *J. Climate*, **30**, 689–702.

Huang G., Hu K. M., and Xie S.-P. (2010). Strengthening of tropical Indian Ocean teleconnection to the northwest Pacific since the mid-1970s: An atmospheric GCM study. *J. Climate*, **23**, 5294–5304

Hurrell, J. W. (1995). Decadal trends in the North Atlantic Oscillation: regional temperatures and precipitation. *Science*, **269**(5224), 676-679.

IPCC (2013). Summary for Policymakers. In: Climate Change 2013: The Physical Science Basis. Contribution of Working Group I to the Fifth Assessment Report of the Intergovernmental Panel on Climate Change [Stocker, T.F., D. Qin, G.K. Plattner, M. Tignor, S.K. Allen, J. Boschung, A. Nauels, Y. Xia, V. Bex, and P.M. Midgley (eds.)]. Cambridge University Press, Cambridge, United Kingdom and New York, NY, USA, pp. 3–29.

Iskandar, I., Masumoto, Y., and Mizuno, K. (2009). Subsurface equatorial zonal current in the eastern Indian Ocean, *J. Geophys. Res*., **114**, C06005.

Izumo, T., Montegut, C. B., Luo, J.-J., Behera, S. K., Masson, S., and Yamagata, T. (2008). The Role of the Western Arabian Sea Upwelling in Indian Monsoon Rainfall Variability. *J. Climate*, **21**, 5603-5623

Izumo, T., J. Vialard, M. Lengaigne, C. de Boyer Montegut, S. K. Behera, J.-J. Luo, S. Cravatte, S. Masson and T. Yamagata, 2010: Influence of the state of the Indian Ocean Dipole on the following year's El Niño. Nature Geosci., 3, 168-172.

Jones, J. M., Gille, S. T., Goosse, H., Abram, N. J., Canziani, P. O., Charman, D. J., Clem, K. R., Crosta, X., de Lavergne, C., Eisenman, I., England, M. H., Fogt, R. L., Frankcombe, R. M., Marshall, G. J., Masson-Delmotte, V., Morrison, A. K., Orsi, A. J., Raphael, M. N., Renwick, J. A., Schneider, D. P., Simpkins, G.

R., Steig, E. J., Stenni, B., Swingedouw, D., and Vance, T. R. (2016). Assessing recent trends in high-latitude Southern Hemisphere surface climate, *Nature Climate Change*, **6**, 917-926.

Jouanno, J., Hernandez, O., and Sanchez-Gomez, E. (2017). Equatorial Atlantic interannual variability and its relation to dynamic and thermodynamic processes. *Earth System Dynamics*, **8**(4), 1061-1069.

Kao, H. Y., and Yu, J. -Y. (2009). Contrasting Eastern-Pacific and Central-Pacific types of ENSO. *J. Climate*, **22**, 615-632.

Karoly, D. J. (1989). Southern Hemisphere circulation features associated with El Niño–Southern Oscillation events. *J. Climate*, **2**, 1239–1252.

Keenlyside, N. S., and Latif, M. (2007). Understanding equatorial Atlantic interannual variability. *J. Climate*, **20**(1), 131-142.

Kerr, R. A. (2000). A North Atlantic climate pacemaker for the centuries. *Science*, **288**(5473), 1984-1985.

Kessler, W. S., Rothstein, L. M., and Chen, D. (1998). The annual cycle of SST in the eastern tropical Pacific, diagnosed in an ocean GCM. *J. Climate*, **11**, 777–799.

Kiladis, G.N., von Storch, H., and Loon, H. (1989). Origin of the South Pacific Convergence Zone. *J. Climate*, **2**, 1185–1195.

Kim, S. T., and Yu, J.-Y. (2012). The two types of ENSO in CMIP5 models, *Geophys. Res. Lett*., **39**, L11704.

Klein, S. A., Soden, B. J, Lau, N.-C. (1999), Remote sea surface temperature variations during ENSO: Evidence for a tropical atmospheric bridge. *J. Climate*, **12**: 917–932.

Knight, J. R., Allan, R. J., Folland, C. K., Vellinga, M., and Mann, M. E. (2005). A signature of persistent natural thermohaline circulation cycles in observed climate. *Geophys. Res. Lett*., **32**(20), L20708.

Kossin, J. P., and Vimont, D. J. (2007). A more general framework for understanding Atlantic hurricane variability and trends. *Bull. Amer. Meteor. Soc.*, **88**(11), 1767-1782.

Kostov, Y., Armour, K. C., and Marshall, J. (2014). Impact of the Atlantic meridional overturning circulation on ocean heat storage and transient climate change. *Geophys. Res. Lett.*, **41**(6), 2108-2116.

Kostov, Y., J. Marshall, U. Hausmann, K. C. Armour, D. Ferreira, and M. M. Holland, 2016. Fast and slow responses of Southern Ocean sea surface temperature to SAM in coupled climate models, *Clim. Dyn*., **48**, 1595-1609.

Kucharski, F., Bracco, A., Yoo, J. H., and Molteni, F. (2007). Low-frequency variability of the Indian monsoon–ENSO relationship and the tropical Atlantic: The “weakening” of the 1980s and 1990s. *J. Climate*, **20**(16), 4255-4266.

Kucharski, F., Bracco, A., Yoo, J. H., & Molteni, F. (2008). Atlantic forced component of the Indian monsoon interannual variability. *Geophys. Res. Lett*., **35**(4), L04706.

Kucharski, F., Bracco, A., Yoo, J. H., Tompkins, A. M., Feudale, L., Ruti, P., and Dell'Aquila, A. (2009). A Gill–Matsuno-type mechanism explains the tropical Atlantic influence on African and Indian monsoon rainfall. *Quarterly Journal of the Royal Meteorological Society,* **135**(640), 569-579.

Kug, J. S., Li, T., An, S. I., et al. (2006), Role of the ENSO–Indian Ocean coupling on ENSO variability in a coupled GCM, *Geophys. Res. Lett*., **33**, L09710.

Kug, J.-S., Jin, F.-F., and An, S.-I. (2009). Two types of El Niño events: Cold tongue El Niño and warm pool El Niño. *J. Climate*, **22**, 1499–1515.

Kwok, R., and Comiso, J. C. (2002). Spatial patterns of variability in Antarctic surface temperature: Connections to the South Hemisphere annular mode and the Southern Oscillation. *Geophys. Res. Lett.*, **29**, L1705.

Lambert, E., Bars, D. L., and de Ruijter, W. P. (2016). The connection of the Indonesian Throughflow, South Indian Ocean Countercurrent and the Leeuwin Current. *Ocean Science*, **12**(3), 771-780.

Larkin, N. K. and Harrison, D. E. (2005). On the definition of El Niño and associated seasonal average U.S. weather anomalies. *Geophys. Res. Lett*., **32**, L13705.

Latif, M., and Barnett, T. P. (1994). Causes of decadal climate variability over the North Pacific and North America. *Science*, **266**, 634–637.

Latif, M., Anderson, D., Barnett, T., Cane, M., Kleeman, R., Leetmaa, A., O'Brien, J., Rosati, A., and Schneider, E. (1998). A review of the predictability and prediction of ENSO, *J. Geophys. Res*., **103**(C7), 14375–14393.

Lau, N. C., and Nath, M. J. (1996). The role of the "atmospheric bridge" in linking tropical Pacific ENSO events to extratropical SST anomalies. *J. Climate*, **9**, 2036–2057.

Lau, N. C. and Nath, M. J. (2004). Coupled GCM simulation of atmosphere-ocean variability associated with zonally asymmetric SST changes in the tropical Indian Ocean. *J. Climate*, **17**, 245–265.

Lee T. (2004). Decadal weakening of the shallow overturning circulation in the South Indian Ocean. *Geophys. Res. Lett.*, 2004, 31(18), L18305.

Lee T. and McPhaden, M. J. (2008). Decadal phase change in large-scale sea level and winds in the Indo-Pacific region at the end of the 20th century. *Geophys. Res. Lett.*, **35**, L01605.

Lee, T., and McPhaden, M. J. (2010). Increasing intensity of El Niño in the central-equatorial Pacific. *Geophys. Res. Lett.*, **37**, L14603.

Legeckis, R. (1977). Long waves in the eastern equatorial Pacific: A view of a geostationary satellite, *Science*, **197**, 1,177 – 1,181.

L'Heureux, M., et al. (2017). Observing and predicting the 2015/16 El Niño. *Bull. Amer. Meteor. Soc.*, **98**, 1363-1382.

Li, C., Wu, L., and Chang, P. (2011). A far-reaching footprint of the tropical Pacific meridional mode on the summer rainfall over the Yellow River Loop Valley. *J. Climate*, **24**, 2585–2598.

Li, T, Wang, B., Chang, C.-P. and Zhang, Y. (2003). A theory for the Indian Ocean dipole–zonal mode. *J. Atmos. Sci.,* **60**, 2119–2135.

Li, T., and Philander, S. G. H. (1996). On the annual cycle of the eastern equatorial Pacific. *J. Climate*, **9**, 2986–2998.

Liang, Y.-C., Yu, J.-Y., Saltzman, E. S., and Wang, F. (2017). Linking the Tropical Northern Hemisphere Pattern to the Pacific Warm Blob and Atlantic Cold Blob, *J. Climate*, **30**, 9041-9057.

Liebmann, B., and Mechoso, C. R. (2011). The South American Monsoon System. The global monsoon system. In: Chang C-P, Ding Y, Lau N-C (eds) The global monsoon system: research and forecast, 2nd edn. World Scientific Publication Company, Singapore, pp 137–157

Linkin, M. E., and Nigam, S. (2008). The North Pacific Oscillation-West Pacific teleconnection pattern: Mature-phase structure and winter impacts. *J. Climate*, **21**, 1979-1997.

Liu, J., Curry, A. J., and Martinson, D. G. (2004). Interpretation of recent Antarctic sea ice variability. *Geophys. Res. Lett*., **31**, L02205.

Liu, Q. Y., Feng, M., Wang, D., et al. (2015). Interannual variability of the I ndonesian T hroughflow transport: A revisit based on 30 year expendable bathythermograph data. *J. Geophys. Res.- Oceans*, **120**(12), 8270-8282.

Lique, C., and Steele, M. (2012). Where can we find a seasonal cycle of the Atlantic water temperature within the Arctic Basin? *J. Geophys. Res*., **117**, C03026.

López-Parages, J., and Rodríguez-Fonseca, B. (2012). Multidecadal modulation of El Niño influence on the Euro-Mediterranean rainfall. *Geophys. Res. Lett.*, **39**(2), L02704.

Losada, T., Rodríguez-Fonseca, B., Mechoso, C. R., and Ma, H. Y. (2007). Impacts of SST anomalies on the North Atlantic atmospheric circulation: a case study for the northern winter 1995/1996. *Clim. Dyn*., **29**(7-8), 807-819.

Losada, T., Rodríguez-Fonseca, B., Polo, I., Janicot, S., Gervois, S., Chauvin, F., and Ruti, P. (2010). Tropical response to the Atlantic Equatorial mode: AGCM multimodel approach. *Clim. Dyn*., **35**(1), 45-52.

Losada, T., Rodríguez-Fonseca, B., and Kucharski, F. (2012). Tropical influence on the summer Mediterranean climate. *Atmospheric Science Letters*, **13**(1), 36-42.

Losada, T., & Rodríguez-Fonseca, B. (2016). Tropical atmospheric response to decadal changes in the Atlantic Equatorial Mode. Clim. Dyn., 47(3-4), 1211-1224.

Ma, C.-C., Mechoso, C. R., Robertson, A. W., and Arakawa, A. (1996). Peruvian stratus clouds and the tropical Pacific circulation: A coupled ocean–atmosphere GCM study. *J. Climate*, **9**, 1635–1645.

Mann, M. E., Zhang, Z., Rutherford, S., Bradley, R. S., Hughes, M. K., Shindell, D., et al. (2009). Global signatures and dynamical origins of the Little Ice Age and Medieval Climate Anomaly. *Science*, **326**(5957), 1256-1260.

Manzini, E., Giorgetta, M. A., Esch, M., Kornblueh, L., and Roeckner, E. (2006). The influence of sea surface temperatures on the northern winter stratosphere: Ensemble simulations with the MAECHAM5 model. *J. Climate*, **19**, 3863–3881.

Marshall, J., Kushnir, Y., Battisti, D., Chang, P., Czaja, A., Dickson, R., et al. (2001). North Atlantic climate variability: phenomena, impacts and mechanisms. *International journal of climatology*, **21**(15), 1863-1898.

Marshall, J., Donohoe, A., Ferreira, D., and McGee, D. (2014). The ocean's role in setting the mean position of the Inter-Tropical Convergence Zone. *Clim. Dyn*., **42**(7-8), 1967-1979.

Martín-Rey, M., Rodríguez-Fonseca, B., Polo, I., & Kucharski, F. (2014). On the Atlantic–Pacific Niños connection: a multidecadal modulated mode. *Clim. Dyn*., **43**(11), 3163-3178.

Mantua, N. J., Hare, S. R., Zhang, Y., Wallace, J. M., and Francis, R. C. (1997). A Pacific interdecadal climate oscillation with impacts on salmon production. *Bull. Amer. Meteor. Soc.*, **78**, 1069-1079.

McCreary, J. P., and Lu, P. (1994). On the interaction between the subtropical and the equatorial oceans: The subtropical cell. *J. Phys. Oceanogr*., **24**, 466 – 497.

McPhaden, M. J., Cronin, M. F., and McClurg, D. C. (2008). Meridional structure of the surface mixed layer temperature balance on seasonal time scales in the eastern tropical Pacific. *J. Climate*, **21**, 3240-3260.

McPhaden, M. J., and Zhang, D. (2002). Slowdown of the meridional overturning circulation in the upper Pacific Ocean. Nature, 415, 603-608.

McPhaden, M. J., and Zhang, D. (2004). Pacific Ocean circulation rebounds. Geophys. Res. Lett., 31, L18301.

McPhaden, M.J., Busalacchi, A.J., Cheney, R., Donguy, J.R., Gage, K.S., Halpern, D., et al., (1998). The Tropical Ocean-Global Atmosphere (TOGA) observing system: A decade of progress. *J. Geophys. Res.* **103**, 14,169-14,240.

McPhaden, M.J., Meyers, G., Ando, K., Masumoto, Y., Murty, V. S. N., Ravichandran, M., Syamsudin, F., Vialard, J., Yu, L., and Yu, W. (2009). RAMA: The Research Moored Array for African-Asian-Australian Monsoon Analysis and Prediction. *Bull. Am. Meteor. Soc.,* **90***,* 459-480.

McPhaden, M. J., Busalacchi, A. J. and Anderson, D. L. T. (2010). A TOGA retrospective. *Oceanography*, **23**, 86-103.

McPhaden, M. J., Lee, T., and McClurg, D. (2011). El Niño and its relationship to changing background conditions in the tropical Pacific Ocean*. Geophys. Res. Lett*., **38**, L15709.

McPhaden, M. J. and Nagura, M. (2014). Indian Ocean Dipole interpreted in terms of Recharge Oscillator theory. *Clim. Dyn*., **42**, 1569–1586.

McPhaden, M. J., Wang, Y., and Ravichandran, M. (2015). Volume transports of the Wyrtki Jets and their Relationship to the Indian Ocean Dipole. *J. Geophys. Res.*, **120**, 5302-5317.

Mechoso, C. R., and Lyons, S. W. (1988). On the atmospheric response to SST anomalies associated with the Atlantic warm event during 1984. *J. Climate*, **1**, 422-428.

Mechoso, C. R., Lyons, S. W., and Spahr, J. A. (1990). The impact of sea surface temperature anomalies on the rainfall over northeast Brazil. *J. Climate*, **3**, 812-826.

Medred, C. (2014). Unusual species in Alaska waters indicate parts of Pacific warming dramatically. *Alaska Dispatch News*, **14** September, http://www.adn.com/article/20140914/unusual-speciesalaska-waters-indicate-parts-pacific-warming-dramatically.

Meehl, G. A., and Arblaster, J. M. (2001). The Tropospheric Biennial Oscillation and Indian Monsoon rainfall, *Geophys. Res. Lett*., **28**, 1731-1734.

Meyers, G., Bailey, R. J., and Worby, A. P. (1995). Geostrophic transport of Indonesian Throughflow, *Deep Sea Res*., **42**(7), 1163 – 1174.

Meredith, M. P. and Hogg, A. M. (2006). Circumpolar response of Southern Ocean eddy activity to changes in the Southern Annular Mode. *Geophys. Res. Lett*., **3**, L16608.

Minobe, S. (1999), Resonance in bidecadal and pentadecadal climate oscillations over the North Pacific: Role in climatic regime shifts, *Geophys. Res. Lett*., **26**, 855 – 858.

Miyama T, McCreary Jr J P, Jensen T G, et al. (2003). Structure and dynamics of the Indian-Ocean cross-equatorial cell. *Deep Sea Research Part II: Topical Studies in Oceanography*, **50**(12-13), 2023-2047.

Mo, K. C., 2000: Relationships between interdecadal variability in the Southern Hemisphere and sea surface temperature anomalies. *J. Climate*, **13**, 3599–3610.

Mo, K. C. and Livezey, R. E. (1986). Tropical-extratropical geopotential height teleconnections during the Northern Hemisphere winter. *Mon. Wea. Rev*., **114**, 2488-2515

Mohino, E., Janicot, S., & Bader, J. (2011). Sahel rainfall and decadal to multi-decadal sea surface temperature variability. *Clim. Dyn*., **37**(3-4), 419-440.

Murakami, H., and Coauthors (2017). Dominant role of subtropical Pacific warming in extreme eastern Pacific hurricane seasons: 2015 and the future. *J. Climate*, **30**, 243–264.

Myers, T. A., C. R. Mechoso, G. V. Cesana, M. J. DeFlorio, and D. E. Waliser, 2018: Cloud feedback key to marine heatwave off Baja California. *Geophys. Res. Lett.*, **45**.

Neelin, J. D., Battisti, D. S., Hirst, A. C., Jin, F.-F., Wakata, Y., Yamagata, T., and Zebiak, S. E. (1998). ENSO theory. *J. Geophys. Res.*, **103**(C7), 14261–14290.

Newman, M., Shin, S.-I., and Alexander, M. A. (2011). Natural variation in ENSO flavors. *Geophys. Res. Lett*., L14705.

Newman, M., and Coauthors (2016). The Pacific decadal oscillation, revisited. *J. Climate*, **29**, 4399–4427.

Ng, B., Cai, W., and Walsh, K. (2014), The role of the SST-thermocline relationship in Indian Ocean Dipole skewness and its response to global warming, *Sci. Rep.*, **4**, 6034.

Niiler, P.P., A. Sybrandy, K. Bi, P. Poulain and D. Bitterman (1995). Measurements of the water-following capability of Holey-sock and TRISTAR drifters. *Deep Sea Res.*, *Part I*, **42**, 1951-1964.

Nnamchi, H. C., Li, J., & Anyadike, R. N. (2011). Does a dipole mode really exist in the South Atlantic Ocean?. *J. Geophys. Res.-Atmospheres*, **116**(D15).

Nnamchi, H. C., Li, J., Kucharski, F., Kang, I. S., Keenlyside, N. S., Chang, P., & Farneti, R. (2015). Thermodynamic controls of the Atlantic Niño. *Nature communications*, **6**, 8895.

Nnamchi, H. C., Li, J., Kucharski, F., Kang, I. S., Keenlyside, N. S., Chang, P., & Farneti, R. (2016). An equatorial–extratropical dipole structure of the Atlantic Niño. *J. Climate*, **29**(20), 7295-7311.

Nnamchi, H. C., Kucharski, F., Keenlyside, N. S., & Farneti, R. (2017). Analogous seasonal evolution of the South Atlantic SST dipole indices. *Atmospheric Science Letters*, **18**(10), 396-402.

Nobre, P., & Shukla, J. (1996). Variations of sea surface temperature, wind stress, and rainfall over the tropical Atlantic and South America. *J. Climate*, **9**(10), 2464-2479.

Notz, D. and Stroeve, J. (2016). Observed Arctic sea-ice loss directly follows anthropogenic CO2 emission. *Science*, **354**, 747–750.

Nummelin, A., Ilicak, M., Li, C., and Smedsrud, L. H. (2016). Consequences of future increased Arctic runoff on Arctic Ocean stratification, circulation, and sea ice cover, *J. Geophys. Res.-Oceans*, **121**, 617–637.

Okumura, Y., & Xie, S. P. (2004). Interaction of the Atlantic equatorial cold tongue and the African monsoon. *J. Climate*, **17**(18), 3589-3602.

Okumura, Y. M. and Deser, C. (2010). Asymmetry in the duration of El Niño and La Niña. *J. Climate*, **23**, 5826-5843.

Onarheim, I., Eldevik, T., Smedsrud, L.H. and J. C. Stroeve, J. C. (2018). Seasonal and regional manifestation of Arctic sea ice loss, *J. Clim*. **31**, 12, 4917-4932, 2018.

Orsi A. H., Whitworth, T., and Nowlin, W. D. (1995). On the Meridional Extent and Fronts of the Antarctic Circumpolar Current. *Deep-Sea Research I*, **42**(5), 641-673.

Overland, J. E. et al. (2015). The Melting Arctic and Midlatitude Weather Patterns: Are They Connected? *J. Clim*. **28**, 7917-7932.

Overland, J. E., Wang, M. and Salo, S. (2008). The recent Arctic warm period, *Tellus*, **60A**, 589–597

Overland, J., Dunlea, E., Box, J.E., Corell, R., Forsius, M., Kattsov, V., Olsen, M., Pawlak, J., Reiersen, L.-O., Wang, M. (2018). The urgency of Arctic change, *Polar Science*, in press.

Østerhus, S., Woodgate, R., Valdimarsson, H., Turrell, B., de Steur, L., Quadfasel, D., Olsen, S. M., Moritz, M., Lee, C. M., Larsen, K. M. H., Jónsson, S., Johnson, C., Jochumsen, K., Hansen, B., Curry, B.,

Cunningham, S., and Berx, B. (2018). Arctic Mediterranean exchanges: A consistent volume budget and trends in transports from two decades of observations. *Ocean Sci. Discuss*.

Paek, H., Yu, J.-Y. and Qian, C. (2017). Why were the 2015/16 and 1997/98 Extreme El Ninos different? Geophys. Res. Lett., **44**, 1848-1856.

Palóczy A., Gille, S. T. and McClean, J. L. (2018). Oceanic Heat Delivery to the Antarctic Continental Shelf: Large-Scale, Low-Frequency Variability. *J. Geophys. Res. - Oceans*, **123** (11), 7678-7701.

Paolo, F. S., Fricker, H. A., and Padman, L. (2015). Volume loss from Antarctic ice shelves is accelerating, *Science*, **348**, 327-331.

Paolo, F. S., Padman L., Fricker H. A., Adusumilli S., Howard S., Siegfried M.R. (2018). Response of Pacific-sector Antarctic ice shelves to the El Niño /Southern Oscillation. *Nature Geoscience*, **11**, 121-126.

Peterson, B. J., J. McClelland, R. Curry, R. M. Holmes, J. E. Walsh, and K. Aagaard (2006). Trajectory shifts in the Arctic and Subarctic freshwater cycle. *Science*, 313, 1061–1066.

Peterson, W., Robert, M., and Bond, N. (2015). The warm Blob continues to dominate the ecosystem of the northern California Current. *PICES Press*, Vol. 23, No. 2, North Pacific Marine Science Organization, Sidney, BC, Canada, 44–46, https://www.pices.int/publications/pices_press/volume23/PPJuly2015.pdf.

Philander, S. G. H., Gu, D., Halpern, D., Lambert, G., Lau, N.-C., Li, T., and Pacanowski, R. C. (1996). Why the ITCZ is mostly north of the equator. *J. Climate*, **9**, 2958–2972.

Polo, I., Rodríguez-Fonseca, B., Losada, T., and García-Serrano, J. (2008). Tropical Atlantic variability modes (1979–2002). Part I: Time-evolving SST modes related to West African rainfall. *J. Climate*, **21**(24), 6457-6475.

Polvani, L. M., Waugh, D.W., Correa, G. J. P. and Son, S.-W. (2011). Stratospheric ozone depletion: The main drive of Twentieth-Century atmospheric circulation changes in the Southern Hemisphere. *J. Climate,* **24**, 795–812.

Polyakov, I. V., Pnyushkov, A. V., Alkire, M. B., Ashik, I. M., Baumann, T. M., Carmack, E. C., Goszczko, I., Guthrie, J., Ivanov, V. V., Kanzow, T., Krishfield, R., Kwok, R., Sundfjord, A., Morison, J., Rember, R., and Yulin, A. (2017). Greater role for Atlantic inflows on sea-ice loss in the Eurasian Basin of the Arctic Ocean. *Science*, **356**, 285–291

Pritchard, H. D., Ligtenberg, S. R., Fricker, H. A., Vaughan, D. G., van den Broeke, M. R., Padman, L. (2012). Antarctic ice-sheet loss driven by basal melting of ice shelves. *Nature*, **484**, 502–505.

Qu X., and Huang G. (2012). Impacts of tropical Indian Ocean SST on the meridional displacement of East Asian jet in boreal summer. *Int. J. Climatology*, **32**, 2073–2080.

Raphael, M. N. et al. (2016). The Amundsen Sea Low: variability, change, and impact on Antarctic climate. *Bull. Am. Meteorol. Soc.*, **97**, 111–121.

Rasmusson, E. M. and Carpenter, T. H. (1982). Variations in tropical sear surface temperature and surface wind fields associated with the Southern Oscillation/El Niño. *Mon. Wea. Rev.*, **110**, 354-384.

Reppin, J., Schott, F. A., Fischer, J., and Quadfasel, D. (1999). Equatorial currents and transports in the upper central Indian Ocean: Annual cycle and interannual variability. *J. Geophys. Res.*, **104**, 15495-15514.

Rignot, E. and Jacobs, S. S. (2002). Rapid bottom melting widespread near Antarctic Ice Sheet grounding lines. *Science*, **296**, 2020–2023.

Rignot, E., Bamber, J. L., van den Broeke, M. R., Davis, C., Li, Y., van de Berg, W. J. & van Meijgaard, E. (2008). Recent Antarctic ice mass loss from radar interferometry and regional climate modelling. *Nature Geosci*. **1**, 106–110.

Rignot, E., Jacobs, S., Mouginot, J., and Scheuchl, B. (2013). Ice-shelf melting around Antarctica, *Science*, 341, 266–270.

Rodriguez, A., Mazloff, M., and Gille, S. T. (2016). An oceanic heat transport pathway to the Amundsen Sea Embayment*, J. Geophys. Res. - Oceans*, **121**, 3337-3349.

Rodríguez-Fonseca, B., Janicot, S., Mohino, E., Losada, T., Bader, J., Caminade, C. et al. (2011). Interannual and decadal SST-forced responses of the West African monsoon. *Atmospheric Science Letters*, **12**(1), 67-74.

Rodríguez-Fonseca, B., Mohino, E., Mechoso, C. R., Caminade, C., Biasutti, M., Gaetani, M., et al. (2015). Variability and predictability of West African droughts: A review on the role of sea surface temperature anomalies. *J. Climate*, **28**(10), 4034-4060

Roemmich, D, Church, J, Gilson, J, Monselesan, D, Sutton, P, and Wijffels, S. (2015). Unabated planetary warming and its ocean structure since 2006. *Nature Climate Change*. **5**, 240-245.

Rogers, J. C., 1981: The North Pacific Oscillation. *Int. J. Climatology.*, **1**, 39–57.

Ropelewski, C. F. and Halpert, M. C. (1986). North American precipitation and temperature patterns associated with the El Niño/Southern Oscillation. *Mon. Wea. Rev*., **114**, 2352–2362.

Ruiz-Barradas, A., Carton, J. A., & Nigam, S. (2000). Structure of interannual-to-decadal climate variability in the tropical Atlantic sector. *J. Climate*, **13**(18), 3285-3297.

Ruprich-Robert, Y., Msadek, R., Castruccio, F., Yeager, S., Delworth, T., & Danabasoglu, G. (2017). Assessing the climate impacts of the observed Atlantic multidecadal variability using the GFDL CM2. 1 and NCAR CESM1 global coupled models. *J. Climate*, **30**(8), 2785-2810.

Ruprich-Robert, Y., Delworth, T., Msadek, R., Castruccio, F., Yeager, S., & Danabasoglu, G. (2018). Impacts of the Atlantic Multidecadal Variability on North American Summer Climate and Heat Waves. *J. Climate*, **31**(9), 3679-3700.

Saji, N. H., Goswami, B. N., Vinayachandran, P. N., et al. (1999), A dipole mode in the tropical Indian Ocean, *Nature*, **401**, 360-363

Sassi, F., Kinnison, D., Boville, B. A., Garcia, R. R., and Roble, R. (2004). Effect of El Niño–Southern Oscillation on the dynamical, thermal, and chemical structure of the middle atmosphere. *J. Geophys. Res*., **109**, D17108.

Schmidtko, S., Heywood, K. J., Thompson, A. F., Aoki, S. (2014). Multidecadal warming of Antarctic waters, *Science*, **346**, 1227-1231.

Schneider, D.P., Okumura, Y., and Deser, C. (2012). Observed Antarctic interannual climate variability and tropical linkages. *J Climate,* **25**, 4048–4066.

Schott F. A., Mccreary J. P., Johnson G. C. (2004). Shallow overturning circulations of the tropical-subtropical oceans. *Earth's Climate*, **147**, 261-304.

Schott, F. A., Xie, S. P., McCreary J. P. (2009). Indian Ocean circulation and climate variability. *Reviews of Geophysics*, **47**(1).

Seager, R, Hoerling, M., Schubert, S., Wang, H., Lyon, B., Kumar, Nakamura, J., and Henderson, N. (2014). Causes and predictability of the 2011–14 California drought. Assessment Rep., NOAA/OAR/Climate Program Office, 42 pp., http://cpo.noaa.gov/MAPP/californiadroughtreport.

Servain, J., I. Wainer, J. P. McCreary, and A. Dessier (1999), Relationship between the equatorial and meridional modes of climate variability in the tropical Atlantic, Geophys. Res. Lett., 26, 458–488.

Seager, R, Hoerling, M., Schubert, S., Wang, H., Lyon, B., Kumar, Nakamura, J., and Henderson, N. (2015). Causes of the 2011–14 California drought. *J. Climate*, **28**, 6997–7024.

Shao, A., Gille, S. T., Mecking, S., Thompson, L. (2015). Properties of the Subantarctic Front and Polar Front from the skewness of sea level anomaly*, J. Geophys. Res. - Oceans*, **120**, 5179-5193.

Smedsrud, L. H., et al. (2013). The role of the Barents Sea in the Arctic climate system. *Rev. Geophys.*, **51**, 415–449.

Smith, T. M., Reynolds, R. W., Peterson, T. C., & Lawrimore, J. (2008). Improvements to NOAA's historical merged land–ocean surface temperature analysis (1880–2006). *J. Climate*, **21**(10), 2283-2296.

Sokolov, S., and S. R. Rintoul (2009), Circumpolar structure and distribution of the Antarctic Circumpolar Current fronts: 1. Mean circumpolar paths, *J. Geophys. Res*., **114**, C11018.

Spall, M. A. (2011) On the role of eddies and surface forcing in the heat transport and overturning circulation in marginal seas. *J. Climate*, **24**, 4844–4858

Speer, K., Rintoul, S> R., and Sloyan, B. (2000). The Diabatic Deacon Cell. *J. Phys. Oceanogr*., **30**, 3212–3222.

Stammerjohn, S. E., Martinson, D. G., Smith, R. C., Yuan, X., and Rind, D. (2008). Trends in Antarctic annual sea ice retreat and advance and their relation to El Niño-Southern Oscillation and Southern Annular Mode variability. *J. Geophys. Res*., **108**, C03S90.

Stewart, A. L. and Thompson, A. F., 2015. Eddy-mediated transport of warm Circumpolar Deep Water across the Antarctic shelf break. *Geophys. Res. Lett.*, **42**, 432-440.

Sultan, B., and Janicot, S. (2003). The West African monsoon dynamics. Part II: The "preonset" and "onset" of the summer monsoon. *J. Climate*, **16**(21), 3407-3427.

Sutton, R. T., and Hodson, D. L. (2005). Atlantic Ocean forcing of North American and European summer climate. *Science*, **309**(5731), 115-118.

Svendsen, L., Hetzinger, S., Keenlyside, N., & Gao, Y. (2014). Marine-based multiproxy reconstruction of Atlantic multidecadal variability. *Geophys. Res. Lett*., **41**(4), 1295-1300.

Swain, D. L., Tsiang, M., Haugen, M., Singh, D., Charland, A., Rajaratnam, B., and Diffenbaugh, N. S. (2014). The extraordinary California drought of 2013/2014: Character, context, and the role of climate change. *Bull. Am. Meteorol. Soc*., **95**, S3-S7.

Swart, N. C., J. C. Fyfe, E. Hawkins, J. E. Kay, and A. Jahn (2015). Influence of internal variability on Arctic sea-ice trends. Nat. Clim. Change, 5 (2), 86–89.

Swart, N. C., Gille, S. T., Fyfe, J. C., and Gillett, N. (2018). Drivers of Southern Ocean warming and freshening, *Nature Geosci*., **11**, 836-841.

Talley, L. D. (2011). Descriptive physical oceanography: an introduction. Academic Press. Elsevier Science.

Tamsitt, V., Drake, H., Morrison, A. K., Talley, L. D., Dufour, C. O., Gray, A. R., Griffies, S. M., Mazloff, M. R., Sarmiento, J. L., Wang, J., and Weijer, W. (2017). Spiraling up: pathways of global deep waters to the surface of the Southern Ocean. *Nature Communications*, **8**.

Terray, L. (2012). Evidence for multiple drivers of North Atlantic multi-decadal climate variability. *Geophys. Res. Lett*., **39**(19), L19712.

Thompson, D. W. J., Wallace, J. M. and Hegerl, G. C. (2000). Annular modes in the extratropical circulation. Part II: Trends. *J. Climate*, **13**, 1018–1036.

Thompson, D. W. J., Solomon, S., Kushner, P. J., England, M. H., Grise, K. M., and Karoly, D. J. (2011). Signatures of the Antarctic ozone hole in Southern Hemisphere surface climate change, *Nature Geoscience*, **4**(11), 741-749.

Thompson, A. F. and Sallee, J.B. (2012). Jets and topography: Jet transitions and the impact on transport in the Antarctic Circumpolar Current. *J. Phys. Oceanogr.*, **42**, 956-972.

Thompson, R. O. (1984). Observations of the Leeuwin current off Western Australia. *J. Phys. Oceanogr.*, **14**(3), 623-628.

Tozuka, T., Luo, J., Masson, S., et al. (2007), Decadal Modulations of the Indian Ocean Dipole in the SINTEX-F1 Coupled GCM, J. Climate, 20: 2881-2894

Torralba, V., Rodríguez-Fonseca, B., Mohino, E., & Losada, T. (2015). The non-stationary influence of the Atlantic and Pacific Niños on North Eastern South American rainfall. *Frontiers in Earth Science*, **3**, 55

Tulloch, R., Ferrari, R., Jahn, O., Klocker, A., LaCasce, J., Ledwell, J. R., Marshall, J., Messias, Speer, M., and Watson, A. (2014). Direct Estimate of Lateral Eddy Diffusivity Upstream of Drake Passage. *J. Phys. Oceanogr.*, **44**, 2593–2616.

Ummenhofer, C. C., England, M. H., McIntosh, P. C., et al. (2009). What causes southeast Australia's worst droughts?, *Geophys. Res. Lett.*, **36**, L04706.

Ummenhofer, C. C., Biastoch, A., and Böning, C. W. (2017). Multidecadal Indian Ocean Variability Linked to the Pacific and Implications for Preconditioning Indian Ocean Dipole Events, *J. Climate*, **30**, 1739-1751.

Vellinga, M., & Wood, R. A. (2002). Global climatic impacts of a collapse of the Atlantic thermohaline circulation. *Climatic change*, **54**(3), 251-267.

Venegas, S. A., Mysak, L. A., & Straub, D. N. (1997). Atmosphere–ocean coupled variability in the South Atlantic. *J. Climate*, **10**(11), 2904-2920.

Vihma, T. (2014). Effects of Arctic Sea Ice Decline on Weather and Climate: A Review, *Surv Geophys* **35**, 1175–1214.

Villamayor, J., Ambrizzi, T., & Mohino, E. (2018). Influence of decadal sea surface temperature variability on northern Brazil rainfall in CMIP5 simulations. *Clim. Dyn*., **51**(1-2), 563-579.

Vinayachandran, P. N., Saji, N. H., and Yamagata, T. (1999). Response of the equatorial Indian Ocean to an unusual wind event during 1994, *Geophys. Res. Lett.*, **26**: 1613-1616

Walker, G. T., and Bliss, E. W. (1932). World Weather V *Mem. R. Meteorol. Soc*., **4**, 53–84.

Wallace, J. M., and Gutzler, D. S. (1981). Teleconnections in the potential height field during the Northern Hemisphere winter. *Mon. Wea. Rev.*, **109**, 784-812.

Wang Y, and Mcphaden M J. (2017). Seasonal cycle of cross-equatorial flow in the central Indian Ocean. *J. Geophys. Res*., **122**(5).

Webster, P. J., Moore, A. M., Loschnigg, J. P., et al. (1999), Coupled ocean-atmosphere dynamics in the Indian Ocean during 1997-98, *Nature*, *401*, 356-360.

Woodgate, R. A., Aagaard, K., and Weingartner, T. J. (2005). A year in the physical oceanography of the Chukchi Sea: Moored measurements from autumn 1990–1991, *Deep Sea Res., Part II*, **52**, 3116–3149.

Woodgate, R. A., T. Weingartner, and R. Lindsay (2010). The 2007 Bering Strait oceanic heat flux and anomalous Arctic sea-ice retreat, *Geophys. Res. Lett*., **37**, L01602.

Wu, B., Li, T., and Zhou, T. J. (2010). Relative Contributions of the Indian Ocean and local SST anomalies to the maintenance of the western north Pacific anomalous anticyclone during the El Niño decaying summer. *J. Climate*, **23**, 2974-2986

Wu R., Kirtman B. P., and Krishnamurthy V. (2008), An asymmetric mode of tropical Indian Ocean rainfall variability in boreal spring. *J. Geophys. Res*. **113**, D05104.

Wu R., and Yeh, S. W. (2010), A further study of the tropical Indian Ocean asymmetric mode in boreal spring. *J. Geophys. Res*. **115**, D08101.

Wyrtki K. (1973). An equatorial jet in the Indian Ocean. *Science*, **181**(4096). 262-264.

Wyrtki, K. (1981). An estimate of equatorial upwelling in the Pacific, *J. Phys. Oceanogr.*, **11**, 1205-1214.

Xie S.-P., Annamalai H., Schott F. A., McCreary J.P. (2002), Structure and mechanisms of south Indian Ocean climate variability. *J. Climate*, **15**, 867–878.

Xie, S.-P. and Philander, S. G. H. (1994). A coupled ocean-atmosphere model of relevance to the ITCZ in the eastern Pacific. *Tellus*, **46A**, 340-350.

Xie, S.-P., Hu K., Hafner J., Tokinaga H., Du Y., Huang G., and Sampe T. (2009). Indian Ocean capacitor effect on Indo-western Pacific climate during the summer following El Niño. *J. Climate*, **22**, 730–747.

Xie S.-P., Kosaka Y., Du Y., Hu K.M., Chowdary J., Huang G. (2016). Indo-western Pacific Ocean capacitor and coherent climate anomalies in post-ENSO summer: a review. *Adv. Atmos. Sci.,* **33**, 411–432.

Yang, S., Li, Z., Yu, J.-Y., Hu, X., Dong, W., and He, S. (2018). El Niño-Southern Oscillation and Its Impact in the Changing Climate, *National Science Review*, nwy046.

Yang, Y., Li, J. P., Wu, L. X., et al. (2017), Decadal Indian Ocean dipolar variability and its relationship with the tropical Pacific, *Adv. Atmos. Sci*., **34**, 1282-1289.

Yeh, S. W., Kug, J. S., Dewitte, B., Kwon, M. H., Kirtman, B. P., and Jin, F.-F. (2009). El Niño in a changing climate. *Nature*, *461*, 511–514.

Yeo, S. -R., and Kim, K. Y. (2015). Decadal changes in the Southern Hemisphere sea surface temperature in association with El Niño–Southern Oscillation and Southern Annular Mode. *Clim. Dyn.*. 1-16.

Yit Sen Bull, C., and Van Sebille, E. (2016). Sources, fate, and pathways of Leeuwin Current water in the Indian Ocean and Great Australian Bight: A Lagrangian study in an eddy-resolving ocean model*. J. Geophys. Res.-Oceans*, **121**(3), 1626-1639.

You, Y. and Furtado, J. C. (2017). The role of South Pacific atmospheric variability in the development of different types of ENSO, *Geophys. Res. Lett.*, **44** (14), 7438-7446.

Yu., J.-Y., and Mechoso, C. R. (1999). Links between annual variations of Peruvian stratocumulus clouds and of SSTs in the eastern equatorial Pacific. *J. Climate*, **12**, 3305-3318.

Yu, J. Y., Mechoso, C. R., McWilliams, J. C., et al. (2002), Impacts of the Indian Ocean on the ENSO cycle, *Geophys. Res. Lett*., **29**, 46-1-46-4.

Yu, J.-Y. and Lau, K. M. (2004). Contrasting Indian Ocean SST variability with and without ENSO influence: A coupled atmosphere-ocean GCM study. *Meteorology and Atmospheric Physics*, **90**, 179–191.

Yu, J.-Y., Kao, H.-Y., and T. Lee, 2010: Subtropics-Related Interannual Sea Surface Temperature Variability in the Equatorial Central Pacific. *J. Climate*, **23**, 2869-2884.

Yu, J.-Y., Lu, M. M., and Kim, S. T. (2012a). A change in the relationship between tropical central Pacific SST variability and the extratropical atmosphere around 1990. *Enviro. Res. Lett*., **7**, 034025.

Yu, J.-Y., Zou, Y., Kim, St. T., and Lee, T. (2012b). The Changing Impact of El Niño on US Winter Temperatures. *Geophys. Res. Lett*., **39**, L15702.

Yu, J.-Y., Kao, P.-K., Paek, H., Hsu, H.-H., Hung, C.-W., Lu, M.-M., and An, S.-I., (2015a). Linking emergence of the Central-Pacific El Niño to the Atlantic Multi-decadal Oscillation. *J. Climate*, **28**, 651-662.

Yu, J.-Y., Paek, H., Saltzman, E. S., and Lee, T. (2015b). The early-1990s change in ENSO-PSA-SAM relationships and its impact on Southern Hemisphere climate, *J. Climate*, **28**, 9393-9408.

Yu, J.-Y., Wang, X. Yang, S., Paek, H., and Chen, M. (2017). Changing El Niño-Southern Oscillation and Associated Climate Extremes, Book Chapter in Climate Extremes: Patterns and Mechanisms, Wang, S.-Y., Jin-Ho Yoon, Chris Funk, and R. R. Gillies (Ed.), AGU Geophysical Monograph Series, Vol. 226, Pages 3-38.

Yu, J.-Y. and Fang, S. W. (2018). The distinct contributions of the seasonal footprinting and charged-discharged mechanisms to ENSO complexity, *Geophys. Res. Lett*., **45**, 6611-6618.

Yu, L. S., and Rienecker, M. M. (1999). Mechanisms for the Indian Ocean warming during the 1997-98 El Niño, *Geophys. Res. Lett*., **26**, 735-738.

Yuan, D., and Liu, H. (2009). Long-Wave Dynamics of Sea Level Variations during Indian Ocean Dipole Events, *J. Phys. Oceanogr*., **39**, 1115-1132.

Yuan, D., Zhou, H., and Zhao, X. (2013). Interannual Climate Variability over the Tropical Pacific Ocean Induced by the Indian Ocean Dipole through the Indonesian Throughflow, *J. Climate*, *26*, 2845-2861.

Yuan, X., and Li, C. (2008). Climate modes in southern high latitudes and their impacts on Antarctic sea ice, *J. Geophys. Res.*, 113, C06S91.

Yuan, Y., Yang, H., Zhou, W., et al. (2008). Influences of the Indian Ocean dipole on the Asian summer monsoon in the following year, *Int. J. Climatol*., **28**, 1849-1859.

Zaba, K. D., and Rudnick, D. L. (2016). The 2014–2015 warming anomaly in the Southern California Current System observed by underwater gliders. *Geophys. Res. Lett.*, **43**, 1241–1248.

Zebiak, S., 1993: Air–sea interaction in the equatorial Atlantic region. *J. Climate*, **6**, 1567–1586.

Zhan R., Wang Y., Lei X. (2011), Contributions of ENSO and East Indian Ocean SSTA to the interannual variability of Northwest Pacific tropical cyclone frequency. *J. Climate*, **24**, 509-521.

Zhang, H., Clement, A. and Di Nezio, P. (2014). The South Pacific meridional mode: A mechanism for ENSO-like variability. *J. Climate*, **27**, 769-783.

Zhang, R., & Delworth, T. L. (2005). Simulated tropical response to a substantial weakening of the Atlantic thermohaline circulation. *J. Climate*, **18**(12), 1853-1860.

Zhang, R., & Delworth, T. L. (2006). Impact of Atlantic multidecadal oscillations on India/Sahel rainfall and Atlantic hurricanes. *Geophys. Res. Lett*., **33**(17).

Zhang, R., Sutton, R., Danabasoglu, G., Delworth, T. L., Kim, W. M., Robson, J., & Yeager, S. G. (2016). Comment on "The Atlantic Multidecadal Oscillation without a role for ocean circulation". *Science*, **352**(6293), 1527-1527.

Zhang W., Vecchi G. A., Murakami H., Villarini G., Jia L. (2016).The Pacific meridional mode and the occurrence of tropical cyclones in the Western North Pacific. *J Clim*, **29**, 381–398.

Zhang W., Villarini, G., Vecchi G. A. (2017). Impacts of the Pacific meridional mode on June–August precipitation in the Amazon River Basin. *Quat. J. Royal Meteorol Soc*, **143**, 1936–1945.

Zhang, Y., Feng, M., Du, Y., Phillips, H. E., Bindoff, N. L., & McPhaden, M. J. (2018). Strengthened Indonesian Throughflow drives decadal warming in the Southern Indian Ocean. *Geophys. Res. Lett*., **45**, 6167–6175.

Zhao, X., Yuan, D., Yang, G., et al. (2016). Role of the oceanic channel in the relationships between the basin/dipole mode of SST anomalies in the tropical Indian Ocean and ENSO transition, *Adv. Atmos. Sci.*, **33**, 1386-1400.

Zheng, X., Xie, S.-P., Vecchi, G. A., et al. (2010). Indian Ocean Dipole Response to Global Warming: Analysis of Ocean–Atmospheric Feedbacks in a Coupled Model, *J. Climate*, **23**, 1240-1253.

Zhang, Y., Wallace, J. M., and Battisti, D. S (1997). ENSO-like interdecadal variability: 1900-93. *J. Climate*, **10**, 1004-1020.

Zwally J. H. and Gloersen, P. (2008) Arctic sea ice surviving the summer melt: interannual variability and decreasing trend, *Journal of Glaciology*, **54**(185), 279-296.